UNIVERSITY OF THESSALY

SCHOOL OF ENGINEERING

DEPARTMENT OF MECHANICAL ENGINEERING

Postgraduate Thesis

Modeling of gas flow and computation of the effective area in non-rotating piston-cylinder pressure gauges

by

NIKOLAOS VASILEIADIS

Submitted for the Partial Fulfillment

of the Requirements for the Degree of

Master of Science

2017

Εγκρίθηκε από τα Μέλη της Τριμελούς Εξεταστικής Επιτροπής:

Πρώτος Εξεταστής (Επιβλέπων)	Δρ. Βαλουγεώργης Δημήτριος Καθηγητής, Τμήμα Μηχανολόγων Μηχανικών, Πανεπιστήμιο Θεσσαλίας
Δεύτερος Εξεταστής	Δρ. Ανδρίτσος Νικόλαος Καθηγητής, Τμήμα Μηχανολόγων Μηχανικών, Πανεπιστήμιο Θεσσαλίας
Τρίτος Εξεταστής	Δρ. Πελεκάσης Νικόλαος Καθηγητής, Τμήμα Μηχανολόγων Μηχανικών, Πανεπιστήμιο Θεσσαλίας

Certified by the member of the Thesis Committee:

1st member (Supervisor) Dr. Valougeorgis Dimitrios
Professor, Department of Mechanical Engineering, University of Thessaly

2nd member Dr. Andritsos Nikolaos
Professor, Department of Mechanical Engineering, University of Thessaly

3rd member Dr. Pelekasis Nikolaos
Professor, Department of Mechanical Engineering, University of Thessaly

Acknowledgments

I would like to express my gratitude to my supervisor Prof. Dimitris Valougeorgis for investing his trust and support in me and my work related to my thesis. The quality of this thesis has been greatly impacted by their constant support and guidance.

I would like to thank the members of the committee, Prof. Nikolaos Andritsos and Prof. Nikolaos Pelekasis for the time they invested in reading my thesis and providing supportive recommendations. In addition, I am grateful to all my friends and colleagues in the Laboratory of Transport Phenomena and Process Equipment for all the insightful scientific discussions and the good times we had. I would like also to specifically thank Dr. S. Naris for his closed guidance in the implementation of this work.

I would also like to thank my family, Ioannis Vasileiadis, Eleni Eleutheraki and Neoklis Vasileiadis for their continuous support and inspiration. Finally, I would like to express special thanks to my friends for their selfless support.

Modeling of gas flow and computation of the effective area in non-rotating piston-cylinder pressure gauges

Nikolaos Vasileiadis
University of Thessaly, Department of Mechanical Engineering, 2016

Supervisor: Valougeorgis Dimitrios, Professor, Department of Mechanical Engineering, University of Thessaly

Abstract

Piston gauges are considered as primary pressure standards and are frequently used for the calibration of industrial gauges. The need for accurate pressure measurements has always been a major concern in numerous industrial processes and technological applications. Recently however, the interest in high accuracy pressure measurements has been renewed due to their importance in many scientific metrological projects such as the re-determination of the Boltzmann constant and the new determination of the Kelvin unit. In order, to achieve such high accuracy pressure measurements piston gauges are frequently used and great efforts are made to reduce their uncertainties.

This work is focused in the computation of the effective area of non-rotating piston gauges by modeling the gas flow in the piston cylinder gap. At first the different numerical tools that are based either on viscous or kinetic theory for modeling the gas flow inside the gap of piston gauges and the different approaches for the computation of the effective area are presented and benchmarked. Then, the presented methodologies are implemented on dimensional data provided by four different National Metrology Institutes for three FPG8601 configurations and one FRS4 configuration. The pressure distribution inside the piston cylinder gap is determined and the effective area is computed for all configurations based on the viscous and the kinetic approaches. In addition, detailed comparisons between the findings based on the different approaches are provided for all performed simulations. Both viscous and kinetic results for the effective area are also compared with computations provided by Physikalisch-Technische

Bundesanstalt (PTB) for their FPG8601 configuration and the agreement between the compared results is found to be satisfactory. Furthermore, effective area computations from least square approximations of the real dimensional data for all configurations are provided in order to investigate the discrepancies of the implemented approaches.

This study is an additional step in the great efforts made to reduce the uncertainties in the effective area of non-rotating piston gauges due to the gas flow inside the piston cylinder gap in the pressure range of 1- 10^4 Pa.

Μοντελοποίηση ροής αερίου και υπολογισμός ενεργού επιφάνειας σε μετρητές πίεσης μη περιστρεφόμενου εμβόλου

Νικόλαος Βασιλειάδης
Πανεπιστήμιο Θεσσαλίας, Τμήμα Μηχανολόγων Μηχανικών, 2017

Επιβλέπων: Βαλουγεώργης Δημήτριος, Καθηγητής, Τμήμα Μηχανολόγων Μηχανικών, Πανεπιστήμιο Θεσσαλίας

Περίληψη

Η παρούσα εργασία επικεντρώνεται στον υπολογισμό της ενεργού επιφάνειας σε μετρητές εμβόλου μη περιστρεφόμενου εμβόλου μέσω της μοντελοποίησης της ροής αερίου στο διάκενο εμβόλου-κυλίνδρου. Τα συγκεκριμένα όργανα θεωρούνται ως μετρολογικά πρωτογενή πρότυπα και χρησιμοποιούνται αρκετά συχνά στην βαθμονόμηση βιομηχανικών αισθητήρων πίεσης. Ο ακριβής προσδιορισμός της πίεσης αποτελούσε πάντα σημαντικό παράγοντα σε πληθώρα βιομηχανικών διεργασιών και τεχνολογικών εφαρμογών. Πρόσφατα όμως το ενδιαφέρον για μετρήσεις πίεσης υψηλής ακρίβειας έχει ανανεωθεί λόγω του βασικού τους ρόλου σε πληθώρα μετρολογικών ζητημάτων όπως ο επαναπροσδιορισμός της σταθεράς Boltzmann και της μονάδας Kelvin. Προκειμένου να επιτευχθούν μετρήσεις τέτοιας ακρίβειας, συχνά χρησιμοποιούνται μετρητές πίεσης εμβόλου και πρόσφατα γίνεται μεγάλη προσπάθεια για τη μείωση των αβεβαιοτήτων τους.

Αρχικά, παρουσιάζονται και ελέγχονται τα υδροδυναμικά και κινητικά αριθμητικά εργαλεία για την μοντελοποίηση του αερίου στο διάκενό εμβόλου-κυλίνδρου καθώς και οι διαφορετικές προσεγγίσεις υπολογισμού της ενεργού επιφάνειας. Έπειτα, οι παραπάνω μεθοδολογίες εφαρμόζονται σε τρεις μετρητές πίεσης FPG8601 και έναν μετρητή FRS4 των οποίων οι διαστάσεις μετρήθηκαν από τέσσερα διαφορετικά Εθνικά Ινστιτούτα Μετρολογίας. Στην συνέχεια, με βάση τα αριθμητικά εργαλεία που παρουσιάστηκαν προσδιορίζεται η κατανομή της πίεσης μέσα στο διάκενο εμβόλου-κυλίνδρου και υπολογίζεται η ενεργός

επιφάνεια των εν λόγω μετρητικών οργάνων. Επιπλέον, παρουσιάζεται η λεπτομερής σύγκριση των διαφορετικών μεθοδολογιών που χρησιμοποιήθηκαν. Η σύγκριση των υδροδυναμικών και κινητικών αποτελεσμάτων για την ενεργό επιφάνεια δείχνουν ικανοποιητική συμφωνία με υπολογισμούς της PTB που πραγματοποιήθηκαν για τον δικό τους μετρητή πίεσης FPG8601. Τέλος, παρουσιάζονται υπολογισμοί της ενεργού επιφάνειας βασισμένοι σε προσεγγίσεις ελαχίστων τετραγώνων των πραγματικών γεωμετριών, προκειμένου να διερευνηθούν οι ασυμφωνίες μεταξύ των διαφορετικών προσεγγίσεων.

Η παρούσα μελέτη αποτελεί ένα επιπλέον βήμα στην μεγάλη προσπάθεια που γίνεται για την μείωση των αβεβαιοτήτων στον προσδιορισμό της ενεργούς επιφάνειας μετρητών πίεσης μη περιστρεφόμενου εμβόλου λόγω της ροής αερίου στο διάκενο εμβόλου-κυλίνδρου για το εύρος πιέσεων 1-10^4 Pa.

Contents

List of Figures

List of Tables

Chapter 1: Introduction

1.1 Basics of metrology

Metrology as a field of science is one of the oldest ones along with mathematics, geometry, astronomy and medicine and its first appearance dates back in 2900 B.C. when the royal Egyptian cubit was carved from black granite as a standard length unit [1]. The cubit was decreed to be the length of the pharaoh's forearm plus the width of his hand and its success as a standardized length is indicated by the base lengths of the pyramids differing less than 0.05%. Other civilizations produced generally-accepted measurement standards, with Roman and Greek architecture based on distinct systems of measurement. However, with the collapse of the empires and the Dark Ages which followed, although, local systems of measurements were common, comparability was difficult and much of measurement knowledge and standardization was lost. Modern metrology has its roots in the French revolution and was based on a political motivation to unify units throughout France. In March 1791 the metre was defined, leading to the creation of the decimal-based metric system in 1795, which established standards for other types of measurements. The metric system was modernized in 1960 with the creation of the International System of Units (SI).

Metrology is defined as "the science of measurement, embracing both experimental and theoretical determinations at any level of uncertainty in any field of science and technology" and its associated concepts are: the definition of units, the physical realization of units, metrological traceability and measurement uncertainty [2]. The most basic concept of metrology is the definition of a unit of measurement. The International System of Units (SI) has seven recognized base units: length, mass, time, electric current, thermodynamic temperature, amount of substance and luminous intensity and all other SI units are derived from combinations of these base units. Since base units are the reference points for all measurements taken in SI, if the reference value changed, all prior measurements would be incorrect. Thus, the importance of reproducible SI units has led to defining base SI units in terms of physical constants. By defining base SI units with respect to physical constants, they are realizable with a higher level of precision and reproducibility. The second most basic concept of metrology is the realization of a unit which is its conversion into reality. The three possible methods of realization are: a physical realization of

the unit from its definition, a highly reproducible measurement as a reproduction of the unit definition and the use of a material object as the measurement standard. Standards (or etalons) are objects, systems, or experiments with a defined relationship to a unit of measurement and are the fundamental reference for a system of weights and measures by realizing, preserving, or reproducing a unit against which measuring devices can be compared. There are three levels of standards in the hierarchy of metrology: primary, secondary, and working standards. Primary standards are of the highest quality and do not reference to any other standards. Secondary standards are calibrated with reference to primary standards. While, working standards are calibrated with respect to secondary standards and are used to calibrate or check measuring instruments or other material measures.

Another important concept is metrological traceability which is the property of a measurement result whereby, the result can be related to a reference through a documented unbroken chain of calibrations, each contributing to the measurement uncertainty. Traceability permits the comparison of measurements while allowing any measurement to be referenced to higher levels of measurements and back to the very definition of the unit. Traceability is most often obtained by calibration, establishing the relationship between an indication on a measuring instrument or secondary standard and the value of the standard. The four primary reasons for calibrations are to provide traceability to ensure that the instrument or standard is consistent with other measurements, to determine accuracy and to establish reliability. Finally, measurement uncertainty is a value associated with a measurement which quantitatively expresses the doubt existing in the measurement. Measurement uncertainty consists of two components: the width of the uncertainty interval and the confidence level which is the likelihood of the true value to falling within the uncertainty interval.

The concepts described above apply to three main overlapping fields of metrology, which are scientific or fundamental metrology, applied, technical or industrial metrology and legal metrology [3]. Scientific metrology is concerned with the establishment of units of measurement, the development of new measurement methods, the realization of measurement standards, and the transfer of traceability from these standards to users in society. Although fundamental metrology is formally undefined, it is considered to be the top level of scientific metrology which strives for the highest degree of accuracy. Applied, technical or industrial metrology is concerned with the application of standards in measurement to manufacturing technologies and

processes, ensuring the suitability of measurement instruments, their calibration and quality control. Although the emphasis in this field is on the measurements themselves, traceability of the measuring device calibration is necessary to ensure confidence of the performed measurements. Industrial metrology is important to a country's economic and industrial development, and the condition of a country's industrial metrology program can indicate its economic status. Finally, legal metrology "concerns activities which result from statutory requirements and concern measurement, units of measurement, measuring methods and instruments". Such statutory requirements may arise from the need for protection of health, public safety, the environment, protection of consumers and fair trade.

In order to ensure conformity and to standardize metrology many international organizations have been established. The Metre Convention established three main organizations that still operate for the standardization of weights and measures. The first is the General Conference on Weights and Measures (CGPM) which acts as the convention's principal decision making body, consisting of delegates from member states and non-voting observers from associate states. The second is the International Committee for Weights and Measures (CIPM) which consists of eighteen individuals, one from each member state of high scientific standing, nominated by the CGPM. This committee advises CGPM on administrative and technical issues. The third one is the International Bureau of Weights and Measures (BIPM) which is located in Sèvres. It provides metrology services for the GCPM and CIPM, houses the secretariat for the organisations and hosts their meetings. The BIPM has also custody of the international prototype kilogram and metre while over the years, prototype metres and kilograms have been returned to BIPM for recalibration. Moreover, new organisations have been established to accommodate modern metrological needs. The International Organisation of Legal Metrology (OIML) is an intergovernmental organisation created in 1995 to promote the global harmonisation of the legal metrology procedures facilitating international trade. The International Laboratory Accreditation Cooperation (ILAC) created in 1977 standardizes accreditation practices and procedures, recognises competent calibration facilities and assisting countries developing their own accreditation bodies. Finally, the Joint Committee for Guides in Metrology (JCGM) is the committee which has created and still maintains two metrology guides: "Guide to the expression of uncertainty in measurement" and "International vocabulary of metrology - basic and general concepts and associated terms".

Although the above organisations ensure conformity to metrological standards in an international level a national measurement system (NMS) is also required in every country. A national measurement system is a network of national metrology institutes, accreditation bodies and calibration laboratories, which set measurement standards, ensure accuracy, consistency, comparability and reliability of measurements made in a country. A national metrology institute's (NMI) role in a country's measurement system is to conduct scientific metrology, realise base units, maintain primary national standards and provide traceability to international standards for a country. Accreditation bodies are responsible for evaluating laboratories by assessing their competence in testing and calibration according to international standards. To ensure objective and technically-credible accreditation, these bodies are independent of other national measurement system institutions. Finally, calibration laboratories are responsible for calibrations of industrial measurement instruments and since these laboratories are accredited they give companies a traceability link to national metrology standards.

Between international metrology organisations and national measurement systems stand regional metrology organizations (RMOs) which are regional associations of NMIs. The European Association of Metrology Institutes (EURAMET) is the European RMO and is one of the six that are recognised within the framework of the CIPM. EURAMET has National Metrology Institutes from 37 countries as members and 78 laboratories from 26 countries as associates. The scope of EURAMET is to develop and disseminate an integrated, cost effective and internationally competitive measurement infrastructure for Europe. To achieve these goals two main tools are used: the European Metrology Research Programme (EMRP) and the European Metrology Programme for Innovation and Research (EMPIR) with more than 100 joint research projects. The work of this thesis is related to the ongoing EMPIR 14IND06 pres2vac "Industrial standards in the intermediate pressure-to-vacuum range" project.

1.2 Introduction to the FPG8601 and FRS4 gauges

Development of pressure balances dates back to the beginning of the nineteenth century and was stimulated by the growth of industrial applications of steam engines and by the need of measuring thermodynamic properties of gases and liquids at different pressures and temperatures [4]. At the moment, the interest in high accuracy pressure measurements has been renewed due

to their importance in many scientific metrological projects such as the re-determination of the Boltzmann constant and the new determination of the Kelvin unit independent from the triple point of water. In order, to achieve such high accuracy pressure measurements piston cylinder assemblies (PCA) are frequently used as primary pressure standards and great efforts are made to reduce their uncertainties.

In this scope, DH Instruments developed the idea of a force balance gauge called the Fixed Pressure Gauge that uses a lubricating gas in order to avoid frictional forces and to center the piston inside the cylinder [5, 6]. In the FPG8601 the piston cylinder assembly is made of tungsten-carbide with a nominal piston area of 10 cm^2. The piston is straight while the cylinder is symmetrically tapered with a typical clearance of 1 μm in the PCA extremities and 6 μm in the PCA center. At Furness Controls the Furness Rosenberg Standard was developed [7, 8]. The elimination of friction between the piston and cylinder in the FRS4 is achieved by a parallelogram suspension system. In the FRS4 the piston and cylinder are made out of invar with a nominal piston area of about 100 cm^2 and a constant gap of 30 μm. Further development at Furness Controls led to the FRS5, where the piston nominal area was reduced to 45 cm^2 while the gap was kept at 30 μm [9].

Uncertainties in non-rotating piston gauges such as the FPG8601 and the FRS4 mainly originate from the dimensional properties of the piston cylinder assembly and the gas flow inside the piston cylinder clearance. NMIs, frequently in collaboration with universities implement numerical tools to model the gas flow and compute the pressure distribution inside the PCA gap in order to determine the piston effective area. These computations enhance the reliability of the piston gauge measurements and complement results of the effective area based on calibrations performed by other primary pressure standards such as liquid manometers.

1.3 The Knudsen number and flow regimes

In rarefied gas flows the parameter that characterizes the flow is the Knudsen number Kn which is defined as the ratio of the mean free path over a length that characterizes the problem and was introduced around 1909 [10]

$$Kn = \frac{\lambda}{L} \tag{1.2.1}$$

In many cases such as shock waves where it is necessary to locally characterize the flow rarefaction the Knudsen number can be defined in a more general way as

$$\mathrm{Kn} = \frac{\lambda}{\varphi}\left|\frac{d\varphi}{dx}\right| \tag{1.2.2}$$

where φ is a flow quantity of the problem. For a single monoatomic gas with a Hard Sphere intermolecular potential the mean free path can be expressed as [11]

$$\lambda = \frac{m}{\sqrt{2}\pi d^2 \rho} \tag{1.2.3}$$

where m is the molecular mass, d is the diameter of the molecule and ρ is the mass density of the gas. The Knudsen number is also related to other important dimensionless flow numbers and can be written as [12]

$$\mathrm{Kn} = \sqrt{\frac{\pi\gamma}{2}}\frac{\mathrm{Ma}}{\mathrm{Re}} \tag{1.2.4}$$

where γ is the specific heat ratio, while Ma and Re are the widely known Mach and Reynolds numbers. Alternatively, instead of the Knudsen number the rarefaction parameter is also commonly used

$$\delta = \frac{PL}{\mu u_0} = \frac{\sqrt{\pi}}{2\mathrm{Kn}} \tag{1.2.5}$$

where P is the gas pressure, μ is the absolute viscosity, $u_0 = \sqrt{2k_B T / m}$ is the most probable velocity of the gas and k_B is the Boltzmann constant. Both the Knudsen number and the rarefaction parameter are measures of gas rarefaction and departure from local equilibrium.

According to the range of the appropriately chosen Knudsen number the flow regimes can be defined as shown in Table 1.

Table 1: Flow regimes with respect to the Knudsen number

Range of Kn	Flow regime	Governing Equations	Numerical approach
$\mathrm{Kn} \to 0$	Continuum (inviscid)	Euler	Typical CFD schemes
$\mathrm{Kn} < 10^{-3}$	Continuum (viscous)	Navier Stokes	
$10^{-3} < \mathrm{Kn} < 10^{-1}$	Slip (viscous)	Navier Stokes with Slip boundary conditions, Generalized equations	
$10^{-1} < \mathrm{Kn} < 10$	Transition (Knudsen)	Boltzmann Kinetic models	Analytical methods, Variational methods, Discrete Velocity Method, Integro-Moment Method Direct Simulation Monte Carlo
$10 < \mathrm{Kn}$	Free molecular	Boltzmann and kinetic models without collisions	Method of characteristics, Test Particle Monte Carlo

When the Knudsen number is small the flow belongs to the continuum or hydrodynamic regime and the classical Euler or Navier Stokes equations with no slip boundary conditions can be applied with high accuracy. As the Knudsen number is increased the flow moves to the slip regime where the no slip boundary conditions fail and the hydrodynamic approach starts to collapse. In the slip regime the Navier Stokes equations can be still applied but must be treated with velocity slip and temperature jump at the boundaries and the slip coefficients used in this approach must computed based on kinetic theory [12]. As the Knudsen number is further

increased and the flow moves to the transition or free molecular flow regimes the Newton, Fourier and Fick transport laws do not hold and the continuum approach completely collapses. In these regimes non equilibrium phenomena that cannot be described based on a macroscopic approach appear and the flow can only be simulated by kinetic theory [13, 14].

The Boltzmann equation, while valid in all flow regimes, is utilized only in the free molecular up to the transition regime due to the high computational cost involved. The solution of the Boltzmann equation is a computationally formidable if not prohibitive task and to overcome this two distinct methods have been developed over the years. The first method is to replace the collision part of the Boltzmann equation with a suitable kinetic model. In order for a model to be acceptable it must satisfy the five independent collision invariants, the H-theorem and must also provide the correct values for the transport coefficients. For single gases the most widely known kinetic model is the BGK model, which satisfies the collision invariants and the H-theorem but cannot provide the correct expressions for the dynamic viscosity and thermal conductivity simultaneously [15]. However, against its shortcomings the BGK model has been successfully used to model a wide range of problems. Another single gas model is the Shakhov kinetic model which satisfies the collision invariants and provides correct expressions for the transport coefficients but it has not yet been proved or disproved that it obeys the H-theorem [16]. Finally, for a single gas the Ellipsoidal model satisfies all the collision invariants, obeys the H-theorem, and provides the correct expressions for the transport coefficients, however, it is more complicated computationally [17]. For polyatomic gases the Holway [18] and Rykov [19] models are applied while the McCormak [20] model is used for gas mixtures. The above kinetic models are frequently solved by applying the Discrete Velocity Method.

The second method developed to overcome the computationally intensive solution of the Boltzmann equation is to replace it with a stochastic process, namely the Direct Simulation Monte Carlo method [21]. In this stochastic method the physical space of the flow is discretized and a large number of simulating particles are initially uniformly distributed with each particle simulating a large number of real particles. The real motion of the particles is divided into two separate parts. In the first part the particles move without colliding based on their molecular velocity and the determined time step, while in the second part the particle collisions are simulated stochastically. Then, the macroscopic quantities of interest are calculated by sampling

the properties of the simulator particles for a large number of time steps. It is noted that like all stochastic methods the DSMC suffers from statistical noise, especially in slow moving flows.

1.4 Thesis structure and objectives

Pressure measurements play a vital role in numerous industrial processes such as in pharmaceutical, petrochemical or energy production industries to only name a few. The demand for traceable pressure measurements originating from the end users in Europe have been predominantly covered by hundreds of calibrating laboratories accredited by national accreditation bodies. However, over the last decade the advancements made in pressure measurement instrumentation in accredited laboratories has produced a need for new, more accurate primary and secondary pressure standards in the range from approximately 1 Pa up to 10^4 Pa to provide traceability of the pressure measurements to the SI units with a high level of accuracy. Thus the thesis aim is to simulate the gas flow inside the gap of PCAs held by different NMIs based on various approaches and provide a detailed comparison of the findings. The "in-house" kinetic codes implemented here, have been already developed over the years in the Laboratory of Transport Phenomena. The thesis is outlined as follows:

- In Chapter 2 the literature review is presented. It includes the classification and operating principals of pressure measuring instruments and standards as well as their measuring range. Moreover, a more detailed description for the piston-type pressure gauges as well as the tools that can be used to simulate the gas flow inside the piston-cylinder gap of those gauges are provided here.

- In Chapter 3 calculation of the quantity of interest which is the piston effective area assuming a known pressure distribution based on two different approaches is included. The algorithms and commercial software used to compute the pressure distribution along the gap as well as the piston effective area as described above are introduced here. Finally, results for two benchmark cases are provided to ensure the validity of the different approaches.

- In Chapter 4 the dimensional and operational data for the FPG8601 and FRS4 gauges are provided. Moreover, the calculations of the piston effective area for both devices are presented. The results presented above are then compared to determine the discrepancies and uncertainties introduced by the different approaches.

- In Chapter 5 a summary of the thesis with the corresponding concluding remarks are presented.

Chapter 2: Literature review

2.1 Pressure measurement instrumentation

It is well established that pressure measurement is one of the most common in industrial processes and applications and many techniques have been developed since the mid-16th century. Two different terms are used to distinguish the zero reference for a pressure measurement: absolute for a zero referenced pressure measurement against a perfect vacuum or gauge for a zero referenced pressure measurement against ambient air pressure. To distinguish a negative gauge pressure omitting the negative sign the value may be referred as vacuum gauge pressure. Two other useful terms are static and dynamic pressure. Static pressure is the uniform pressure in all directions originating from an immovable fluid, while dynamic pressure is the additional pressure component on a surface perpendicular to the flow direction in a moving fluid. Moreover, an instrument facing the flow direction measures the total or stagnation pressure which is the sum of the two components mentioned above. The instruments used to measure and display pressure above or below the atmospheric are called pressure gauges or vacuum gauges respectively and are separated in two major categories depending on the directness of the measurement [22].

Direct pressures gauges are based on the physical realization of pressure which is the force exerted in a unit area and are further divided in hydrostatic and mechanical gauges. One of the most known hydrostatic gauges is the liquid column gauge (manometer) which consists of a column of liquid in a tube whose ends are exposed to different pressures. The height of the liquid column will change until its weight is in equilibrium with the pressure differential between the two tube ends and thus, the pressure differential can be measured. The preferred working fluids used in these gauges are mercury because of its high density and low vapour pressure, or light oils and water for small pressure differences. The effective pressure range of a simple liquid manometer is between 100 Pa and a few atmospheres. Another hydrostatic gauge is the McLeod gauge which isolates a sample of gas from a vacuum chamber and compresses it by tilting and infilling with mercury. The gas sample pressure is then measured by a mercury manometer and by knowing the compression ration of the gauge the pressure in the original vacuum chamber can be determined. The McLeod gauge has good accuracy and is useful in the range of 10^{-4} Pa up to

10^{-2} Pa, because however the technique is slow, it is unsuited for continual monitoring. Mechanical or aneroid gauges are based on measuring the force exerted on a solid surface or on a solid pressure-sensing element that flexes elastically under the effect of a pressure difference across the element. One of the most commonly used pressure gauges in many industrial or everyday applications is the Bourdon gauge [23]. The Bourdon gauge is a mechanical gauge which uses the principle that a flattened tube tends to straighten when pressurized. In practice, a flattened thin tube with a closed end is connected at the hollow end to a fixed pipe containing the fluid to be measured. As the pressure increases, the closed end moves in an arc, and this motion is converted into rotation of a gear attached to the pointer shaft that indicates the pressure reading. Typical Bourdon gauges can measure between 1 Pa and 60 bar but helical or spiral-type Bourdon gauges can reach up to 7000 bar. A second type of mechanical gauge is the diaphragm pressure gauge that uses the deflection of a flexible ceramic or metallic membrane separating two chambers with different pressures. The deformation of the membrane can be measured using mechanical optical or capacitive techniques in order to have a pressure reading. Diaphragm gauges have also a quite wide pressure measurement range between 10^{-2} Pa and 20 bar. Another category of mechanical gauges are piston-type gauges which measure the force exerted on a piston surface in order to determine the pressure. Piston-gauges are considered as primary standards because however, operating them is elaborate and impractical for everyday measuring tasks particularly in an industrial environment they are mostly used for calibration purposes. Piston-type gauges have a measuring range from 1 Pa up to 1 MPa. Other mechanical gauges are the magnetic level gauge and spinning rotor pressure gauge.

Indirect pressure gauges use known principals in order to measure pressure indirectly. Thermal conductivity pressure gauges measure pressure indirectly based on the fact that as the density of a gas is increased its ability to conduct heat increases. The Pirani sensor is a thermal conductivity gauge that consists of a metal wire filament facing the pressure that is being measured. The wire is heated by an electrical current flowing through and is cooled by the surrounding gas. The equilibrium temperature of the wire, which is the result of the two heat transfer mechanisms, is determined by measuring its electrical resistance and thus the gas pressure can be determined. Pirani gauges pressure measurements range between 0.1 Pa and 10 kPa. Other thermal conductivity gauges such as the thermocouple or thermistor gauges are based on exactly the same principal. However they use a thermocouple or thermistor respectively to

measure the temperature of the heated wire directly and their measurement range lies between 0.1 and 100 Pa. Ionization gauges are the most sensitive gauges and are used for very low pressures between 0.1 Pa and 10^{-8} Pa referred as hard or high vacuum [24]. They measure pressure indirectly exploiting the fact that gas ionization effects are pressure dependent. There are several sub-categories of ionization gauges which can be separated in two distinct types. The first type is the emitting-cathode or hot-cathode ionization gauge that uses an electrically heated filament to produce the electron beam which ionizes the surrounding gas. The resulting ions are collected at a negative electrode and the produced ion current is measured in order to determine the pressure of the gas. The second type are the crossed-field ionization gauges which use a gas discharge between two metal electrodes by applying sufficiently high voltage. The discharge current is pressure dependent and thus it is used as the measured quantity.

2.2 Piston-cylinder pressure gauges

Since 1990s, piston gauges and so-called pressure balances are considered as primary standards as they provide uncertainties of only a few 10^{-6} in the range of 2 kPa and 300 kPa [22]. As shown in Fig. 1 a gas operated piston gauge consists of a rotating cylindrical piston closely fitted in a circular cylinder. The gap width between the piston-cylinder assembly is typically between a couple of micrometers and a few tenths of micrometers. The piston gauge generates a pressure difference between the piston bottom and the volume above the piston-cylinder assembly. The enclosed volume can be maintained at atmospheric pressure in order to get a gauge pressure measurement or can be evacuated to get an absolute measurement. In the rotating piston configuration the rotational movement is necessary to maintain the piston centered while minimizing friction effects. The correct measurement for the pressure at the base of the piston is defined as the total downward force on the piston, which is defined solely on the weight of the piston and the additional masses, to the effective area of the piston. The effective area of the piston can be determined by dimensional measurements, or if the weight is known, from pressure comparison with liquid manometers. Comparisons with liquid manometers are far more convenient and more precise in determining the piston area because disturbing effects such as misalignments of the piston axis, eccentricities of the part and friction effects are calibrated into the effective area. Moreover, possible influences of gas species, operating height and

pressure on the effective area are easily determined by comparison with liquid manometers. However, since the mid-1990s, it has been made possible to consider these aspects in calculations and to manufacture piston-cylinder assemblies with great dimensional accuracy that can provide high accuracy metrological measurements.

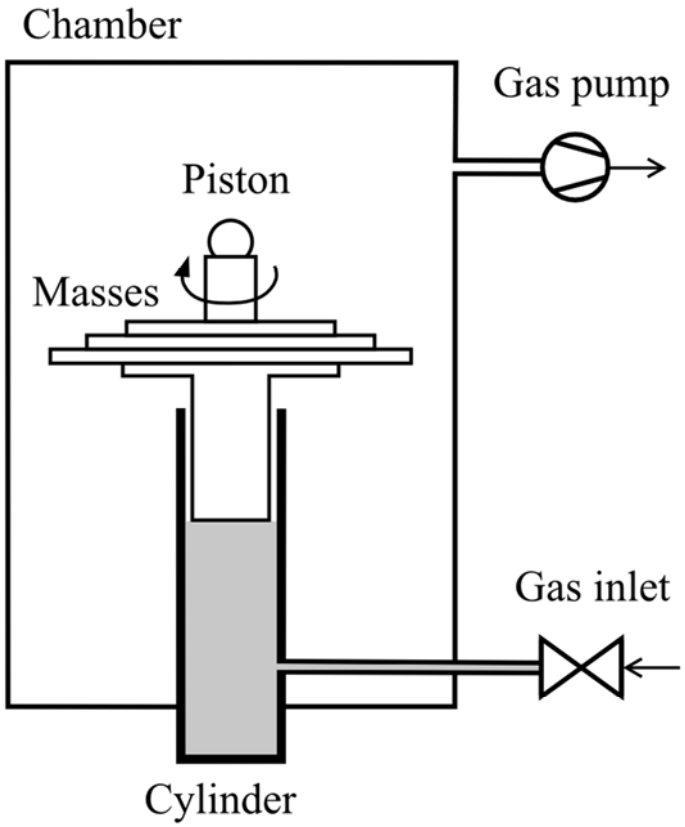

Figure 1: Schematic diagram of a rotating piston gauge.

In the late 1990s the so-called pressure balances became commercially available. In contrast to the principle of a rotating piston gauge, however, the force exerted by the gas is not measured by masses placed on top of the piston but by a balance (force meter). This design prevents the centering of the piston by rotation, since the force exerted on the piston must be transferred to the balance by a steady connection. In addition the clearance between the piston and the cylinder needs to be larger than that of a rotating piston gauge in order to avoid static frictional forces.

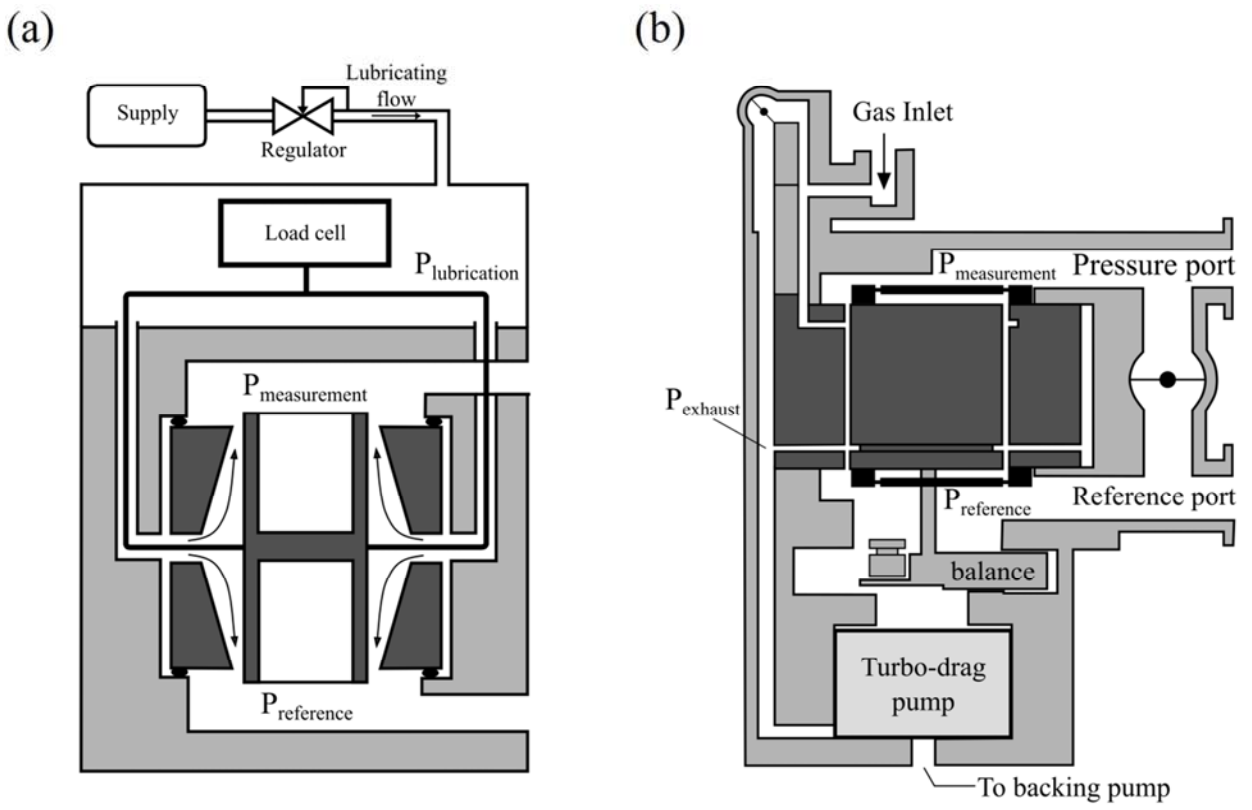

Figure 2: Schematic diagram of (a) an FPG8601 piston gauge; (b) an FRS4 piston gauge.

In Fig. 2a a diagram of the FPG8601 is presented. The FPG8601 is based on the configuration proposed in [5, 6]. In this setup the piston and cylinder are both manufactured from tungsten-carbide and the pressure range is from 1 Pa up to 15000 kPa. As shown in Fig. 2a the working volume and the reference pressure volume are placed above and below the piston cylinder assembly respectively, unlike the configuration of the typical rotating piston gauge. The FPG8601 can be operated in gauge and absolute mode and the reference chamber is equipped with a turbo-molecular and a rotary vane pump in order to maintain the desired vacuum. The piston, which has a nominal area of 10 cm^2, is held at the center of the cylinder with an equal conical gap, which has a width of 6 μm at the piston center and reduces symmetrically to 1 μm towards the piston extremities. In order to center the piston and avoid mechanical complexity dry air or N_2 is used as an independent lubricating gas. The gas flows through the load cell chamber and the connecting system piston load cell passage located at the center of the cylinder towards the two pressure chambers. The lubricating gas pressure is controlled by a flow restriction and is set 40 kPa higher than the reference chamber pressure.

In Fig. 2b a diagram of the FRS4 developed by Furness Controls is shown [7]. In this configuration the piston and the cylinder are both made from Invar, a low expansion nickel-iron alloy. The piston with a 100 cm^2 area is held at the center of the cylinder, with an equal gap of about 30 μm all around. The positioning of the piston is maintained with a parallelogram support system of flexible hinges, with one end mounted on the piston and the other end attached to the cylinder. The range of the FRS4 was initially up to 3.2 kPa but has been later extended to 7 kPa [8]. Similar to the FPG configuration the measurement pressure chamber and the reference pressure chambers are located above and below the piston cylinder assembly respectively. The FRS4 can be operated in gauge and absolute modes and the reference port is connected to two vacuum pumps, a hybrid turbo-molecular and a triple drag pump backed up by a small diaphragm pump required to maintain the required vacuum. The gas, which is usually dry air or N_2, flows from the gas inlet inside the piston-cylinder gap and is taken out of the clearance before reaching the reference volume. Thus the reference pressure in absolute mode can be maintained at 10^{-3} Pa for the lower pressure measurement range and no more than 10^{-2} Pa above 2 kPa. Further research at Furness Controls led to the development of FRS5 which follows the same working principal as the FRS4 [9]. However, the piston area has been reduced to 45 cm^2 and the pressure range has been extended up to 11 kPa while the gap was kept constant at 30 μm. Moreover, the possibility to check the zeroing of the instrument without evacuation and an additional turbo molecular pump connected to the working volume have been added to the FRS5.

2.3 Gas flow modeling tools in the gap of a piston gauge

As already mentioned a pressure balance piston gauge operating principal is to measure the net force exerted on the piston by the reference and measurement pressure chambers and then to translate this force measurement into a pressure measurement based on the piston area. However, in the piston-cylinder clearance the gas flow creates additional forces that affect the accuracy of the pressure measurement.

A survey of tools that have already been applied or can be applied to model the lubricating gas flow and to compute the piston effective area is provided. For a PCA with a sufficiently small ratio of the gap width over the piston radius and a sufficiently large ratio of the gap length over the gap length over the gap width the gas flow in the annular gap can be considered as a one

dimensional fully developed flow between two infinite plates. Moreover if the gas flow is assumed to be in the viscous regime Dadson theory can be applied [25]. Dadson theory has been implemented in numerous cases to model the piston-cylinder gas flow and estimate the effective area [26-28]. The well-known flow configuration is shown in Fig. 3 for completeness purposes.

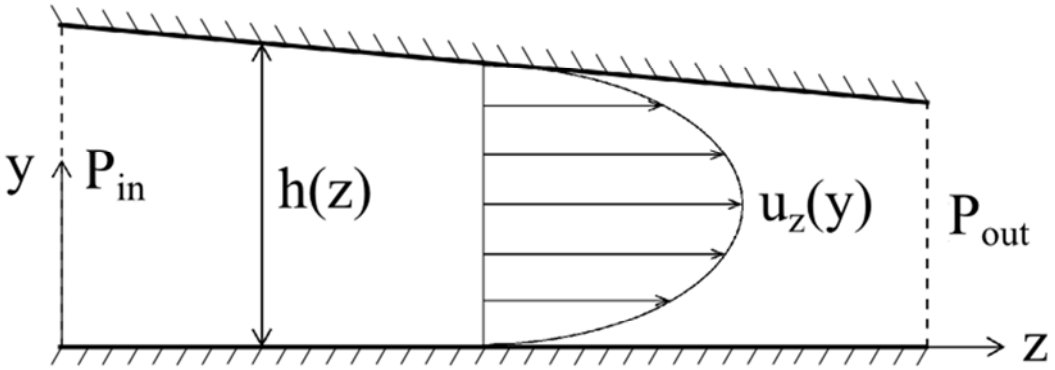

Figure 3: Flow configuration for 1D axial viscous flow.

The velocity field for a certain cross section of the channel is given as

$$u_z(x) = \frac{1}{2\mu}\frac{dP}{dz}y\left(y-h\right) \qquad \text{(Eq. 2.3.1)}$$

where μ is the gas viscosity, P is the gas pressure and h is the gap height. Integrating along the gap height and substituting the gas density using the Ideal gas law the mass flow rate per unit of depth length can be determined as

$$\frac{\dot{M}}{L} = \frac{\rho}{12\mu}\left(-\frac{dP}{dz}\right)h^3 = \frac{P}{12\mu R_g T}\left(-\frac{dP}{dz}\right)h^3 \qquad \text{(Eq. 2.3.2)}$$

where ρ is the gas density, R_g is the specific gas constant and T is the gas temperature. Finally, because the mass flow rate along the channel is constant the ordinary differential equation for the pressure can be solved to provide the pressure expression in a closed form:

$$P^2(z) = P_{in}^2 - \left(P_{in}^2 - P_{out}^2\right)\frac{\int_0^z h^{-3}dz}{\int_0^L h^{-3}dz} \quad \text{(Eq. 2.3.3)}$$

Due to the accuracy required in the gas flow modeling inside the piston-cylinder clearance, two dimensional viscous models have also been applied in [29]. In addition, commercial software such as ANSYS Fluent can be implemented to complement the results provided by the one-dimensional fully developed flow model and to possibly validate its assumptions. ANSYS Fluent is a state-of-the-art computer program written in the C programming language for modeling fluid flow, heat transfer and chemical reactions in complex systems [30]. Complex geometries can be designed by the two build-in features SpaceClaim and DesignModeler or can be imported directly from a variety of CAD programs such as AutoCAD, Solidworks and Pro/Engineer. The discretization of the geometry can be accomplished by the default Fluent mesh generation algorithm or can be imported directly from external meshing programs such as GAMBIT, GeoMesh and TGrid. For all flows, Fluent solves the conservation equations for mass and momentum while for flows involving heat transfer or compressibility an additional equation for the conservation of energy is solved. The equation of mass conservation, or continuity equation, for can be written as

$$\frac{\partial \rho}{\partial t} + \nabla \cdot \left(\rho \vec{u}\right) = 0 \quad (2.3.4)$$

where ρ is the density and $\vec{u}$ is the velocity vector. Momentum conservation in an inertial (non-accelerating) reference frame is given as

$$\frac{\partial \left(\rho \vec{u}\right)}{\partial t} + \nabla \cdot \left(\rho \vec{u}\vec{u}\right) = -\nabla P + \nabla \cdot \left(\bar{\bar{\tau}}\right) + \rho \vec{g} + \vec{F} \quad (2.3.5)$$

where P is the static pressure, $\rho\vec{g}$ and $\vec{F}$ are the gravitational body force and external body forces respectively and $\bar{\bar{\tau}}$ is the stress tensor, which is described as

$$\bar{\bar{\tau}} = \mu\left[\left(\nabla\vec{u} + (\nabla\vec{u})^{T}\right) - \frac{2}{3}(\nabla\cdot\vec{u})I\right] \tag{2.3.6}$$

where μ is the molecular viscosity and I is the unit tensor. For heat transfer or compressible flows Fluent also solves the energy equation in the following form:

$$\frac{\partial(\rho E)}{\partial t} + \nabla\cdot\left(\vec{u}(\rho E + P)\right) = \nabla\cdot\left(\kappa\nabla T + \bar{\bar{\tau}}\cdot\vec{u}\right) + S_h \tag{2.3.7}$$

Here, $E = h - \frac{P}{\rho} + \frac{u^2}{2}$ is the energy, h is the sensible enthalpy, κ is the thermal conductivity, T is the temperature and S_h includes the heat inserted into the system from chemical reactions or any other volumetric heat sources. For the solution of the described equations Fluent can implement either a density-based or a pressure-based solver. The density-based solver solves the governing equations of continuity, momentum and energy simultaneously while governing equations for additional scalars are solved afterwards and sequentially. Because the governing equations are non-linear and coupled several iterations are performed before a converged solution is obtained. Each iteration of the algorithm consists of the following steps:

1. Update the fluid properties based on the current solution. In the first iteration the fluid properties will be updated based on the initialized solution.
2. Solve the continuity, momentum, and energy equations simultaneously.
3. Solve equations for scalars such as turbulence and radiation using the previously updated values of the other variables.
4. Check for convergence of the equation set.

The pressure-based solver uses two different solution algorithms. The segregated algorithm solves the individual governing equations sequentially. The segregated algorithm is memory-efficient, yet the solution convergence is relatively slow, since the equations are solved in a decoupled manner. With the segregated algorithm each iteration is outlined as follows:

1. Update fluid properties based on the current solution. In the first iteration the fluid properties will be updated based on the initialized solution.
2. Solve the momentum equations, sequentially, using the recently updated values of pressure and face mass fluxes.
3. Solve the pressure correction equation using the recently obtained velocity field and the mass-flux.
4. Correct face mass fluxes, pressure, and the velocity field using the pressure correction equation.
5. Solve equations for scalars such as turbulence and radiation using the previously updated values of the other variables.
6. Check for the convergence of the equations.

Unlike the segregated algorithm described above, the pressure-based coupled algorithm solves a coupled system of the pressure-based continuity equation and the momentum conservation equations. Thus, the described Steps 2 and 3 of the segregated algorithm are replaced by a single step in which the coupled system of equations is solved while the remaining equations are solved sequentially. Since, the momentum and continuity equations are solved in a closely coupled manner, the rate of solution convergence significantly improves. However memory allocation is increased as the discrete system of the coupled equations needs to be stored in the memory when solving for the velocity and pressure fields. For the post-processing of the converged solution results Fluent provides various reporting and plotting tools for almost all quantities of interest. Finally Fluent can also export the simulation results in appropriate file formats in order to be post-processed by external software.

In typical PCAs the flow can be partially or fully in the slip regime in the gauge operation mode and even in the free molecular regime in the absolute operation mode. To overcome this problem interpolating formulas connecting the viscous solution with the free molecular regime solution have been used in the past [31-35]. Furthermore, recently planar Poiseuille flow based on kinetic modeling has been implemented in the work by [36, 37]. However, it is well established that in planar geometry when the rarefaction parameter tends to zero the Poiseuille coefficient [38, 39] tends to infinity and thus numerical treatment of the solution is required. In order to circumvent this problem, the concentric annulus Poiseuille flow based on kinetic

modeling can be considered [40]. The flow configuration is shown in Fig. 4 where two vessels maintained at pressures P_{in} and P_{out} with $P_{in} > P_{out}$ are connected via a long concentric annulus with inner and outer radii R_1 and R_2 respectively.

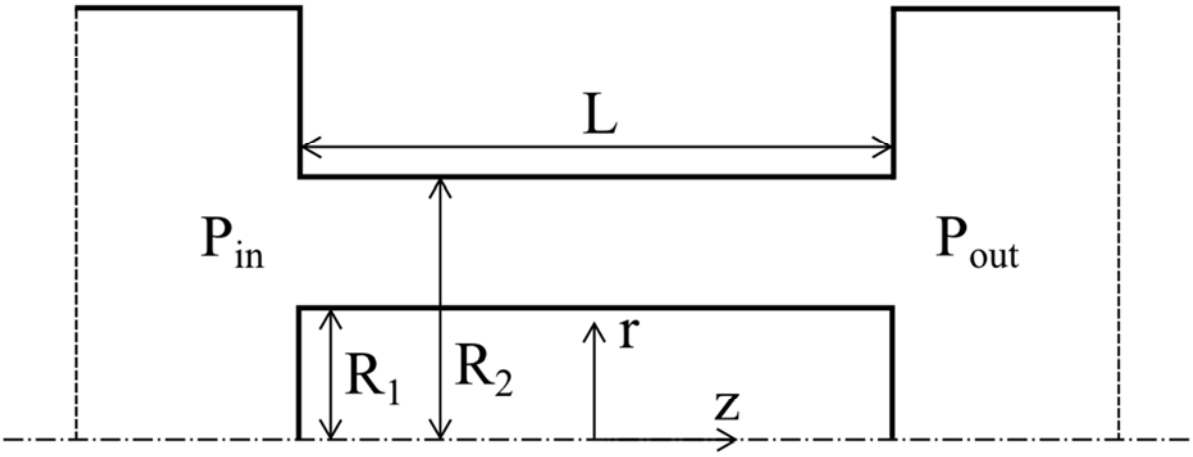

Figure 4: Configuration of a pressure driven flow through a concentric annulus.

The main dimensionless flow parameter is the rarefaction parameter, defined as

$$\delta = \frac{D_h P}{\mu_0 u_0} \tag{2.3.8}$$

where $D_h = 2(R_2 - R_1)$ is the hydraulic diameter, $P = (P_{in} + P_{out})/2$ is a reference pressure, μ_0 is the gas dynamic viscosity at reference temperature T_0 and u_0 is the most probable molecular velocity. In addition, it is convenient to introduce the dimensionless spatial variables $r = r'/D_h$, $z = z'/D_h$ of the problem and also the dimensionless cross section $A = A'/D_h^2$ and perimeter $\Gamma = \Gamma'/D_h$. Since the flow is a pressure driven isothermal flow the BGK kinetic model subject to Maxwell diffuse boundary conditions can be applied. In addition since the flow is fully developed the BGK model can be linearized by considering the dimensionless local pressure gradient, defined as

$$X_P = \frac{D_h}{P}\frac{dP}{dz'} = \frac{1}{P}\frac{dP}{dz} \tag{2.3.9}$$

By introducing the dimensionless quantities and applying the widely used projection procedure the projected linearized BGK model reduces to

$$\zeta\left[\cos\theta\frac{\partial\varphi}{\partial r} - \frac{\sin\theta}{r}\frac{\partial\varphi}{\partial\theta}\right] + \delta\varphi = \delta u - \frac{1}{2} \tag{2.3.10}$$

subject to

$$\varphi(r_1,\zeta,\theta) = 0 \quad \theta\in\left(-\frac{\pi}{2},\frac{\pi}{2}\right), \quad \varphi(r_2,\zeta,\theta) = 0 \quad \theta\in\left(\frac{\pi}{2},\frac{3\pi}{2}\right) \tag{2.3.11}$$

where φ is the reduced distribution function, ζ is the magnitude of the molecular velocity, θ is the polar angle and u is the non-dimensional macroscopic velocity given as

$$u = \frac{u'}{u_0 X_P} = \frac{1}{\pi}\int_0^{2\pi}\int_0^{\infty}\varphi e^{-\zeta^2}d\zeta d\theta \tag{2.3.12}$$

The main macroscopic quantity of practical interest is the mass flow rate through the annulus

$$\dot{M} = \iint_{A'}\rho u' dA' = G\frac{A'D_h}{u_0}\frac{dP}{dz'} \tag{2.3.13}$$

where is G the dimensionless flow rate depending only on the rarefaction parameter δ and the radius ratio R_1/R_2, written as

$$G = \frac{4}{r_2^2 - r_1^2}\int_{r_1}^{r_2} u(r)dr \tag{2.3.14}$$

In the kinetic approach it is clear that when the inlet and outlet pressures are known an iterative procedure for the mass flow rate is required to determine the pressure distribution along the annulus length.

Chapter 3: Effective area of a piston-cylinder gauge

3.1 Calculation of the piston effective area

As already mentioned the most important quantity of a piston gauge is its effective area. The definition of the effective area of a piston-cylinder assembly is given as

$$A_0 = \frac{F_{total}}{\Delta P} \tag{3.1.1}$$

where F_{total} is the total force exerted on the piston and ΔP is the pressure differential between the two gap ends. In order to compute the effective are of a piston cylinder assembly it is required to take into account all the forces that act on the piston.

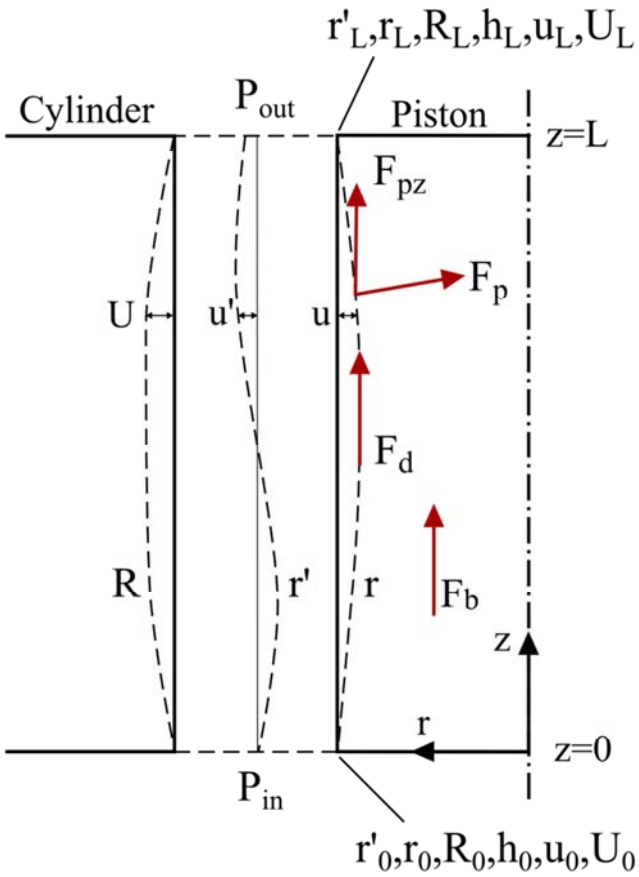

Figure 5: Schematic diagram of piston-cylinder assembly cross section.

Any piston cylinder assembly cross section can be represented as shown in Fig. 5. The chambers below and above the piston are maintained at constant pressure P_{in} and P_{out} respectively with $P_{in} > P_{out}$ and pressure differential $\Delta P = P_{in} - P_{out}$. The piston and cylinder radii are denoted with r and R respectively, while the gap width is $h = R - r$. The neutral surface of the fluid column is denoted with r'. All dimensional data at the gap entrance are denoted by the subscript 0, while at the gap exit the subscript L is used. In addition, u, U and u' are the deviations of the piston, cylinder and neutral surface radii from r_o, R_o and r_0' respectively. Once the dimensional data for the gap are known the piston effective area can be determined as the sum of three terms:

$$A_{0,E} = \left(F_b + F_d + F_{pz}\right) / \Delta P = A_{1,E} + A_{2,E} + A_{3,E} \tag{3.1.2}$$

It is clear that each of the three areas is associated with one of the forces that act on the piston. The first term is associated to the force acting on the piston due to the pressure differential and is written as

$$A_{1,E} = \frac{\pi}{\Delta P}\left(r_0^2 P_{in} - r_L^2 P_{out}\right) \tag{3.1.3}$$

The second term corresponds to the drag force due to the lubricant gas flow through the gap. The drag force acting on the piston surface can be obtained from a force balance equation and the corresponding area is expressed as

$$A_{2,E} = -\frac{\pi}{\Delta P}\int_0^L r(z)\, h(z) \frac{dP}{dz} dz \tag{3.1.4}$$

The expression for the second term is valid for all flow regimes and since $dP/dz < 0$ it is always positive. The third term is related to the pressure force due to the variation of the piston radius:

$$A_{3,E} = \frac{2\pi}{\Delta P}\int_0^L p(z)r(z)\frac{dr}{dz}dz \tag{3.1.5}$$

The third term can be either positive or negative depending on the piston radius curvature along the engagement length of the piston cylinder assembly. In [25] an alternative formulae for the effective area has been derived by equating the forces acting on the annular fluid column between the piston and the neutral surface. The total force acting on the piston is expressed as:

$$F_{total} = \pi r_0'^2\left(P_{in} - P_{out}\right) + 2\pi\int_0^L r'\left(P - P_{out}\right)\frac{du'}{dx}dx \tag{3.1.6}$$

Then the effective area of the piston can be written with respect to the PCA neutral surface radius as

$$A_{0,A} = \pi r_0'^2 + \frac{2\pi}{\Delta P}\int_0^L r'\left(P - P_{out}\right)\frac{du'}{dx}dx \tag{3.1.7}$$

The evaluation of A_0 using the exact value of $r' = \left(R^2 - r^2\right)/\left(2\ln\left(R/r\right)\right)$ would lead to unnecessarily complicated expressions. In [25] the neutral surface radius is approximated by $r' = \left(rR\right)^{1/2}$ and the effective area is easily reduced to

$$A_{0,A} = \pi r_0^2\left(1 + \frac{h_0}{r_0} + \frac{\pi}{r_0\Delta P}\int_0^L\left(P - P_{out}\right)\frac{d\left(u+U\right)}{dx}dx\right) \tag{3.1.8}$$

An equivalent expression derived from Eq. (3.1.8) by integration by parts is written as

$$A_{0,A} = A_{1,A} + A_{2,A} = \pi r_0^2\left(1 + \frac{h_0}{r_0} - \frac{\pi}{r_0\Delta P}\int_0^L\left(u+U\right)\frac{dP}{dx}dx\right) \tag{3.1.9}$$

where $A_{1,A}$ is the piston area at the gap entrance and $A_{2,A}$ is the contribution of the gas flow and the piston curvature to the effective area. It is clear that Eq. (3.1.2) is an exact approach to the calculation of the effective area, while Eq. (3.1.9) is an approximate one. It is noted however that, in Eq. (3.1.9) the derivative of the piston radius is omitted which highly increases its robustness. In the present work both Eqs. (3.1.2) and (3.1.9) are used to calculate the effective area of the piston-cylinder assemblies under investigation.

3.2 Determination of the pressure distribution

All quantities that appear in the computation of a PCA effective area depend only on the piston radius, the cylinder radius and the pressure along the gap. The piston and cylinder dimensional data are provided by the dimensional analysis of the PCA which is usually performed by the corresponding National Metrology Institute. The dimensional analysis provides both the roundness and straightness data of the PCA. The roundness analysis includes the radii of the piston and the cylinder every few degrees for several height positions, while the straightness analysis includes the piston and cylinder radii every few hundreds of micrometers for several angle positions. In the present work the computation domain of the gap is discretized based on the dimensional measurements, where each node corresponds to an individual dimensional measurement along the gap.

It is clear that once the dimensional data of the PCA along with the inlet and outlet pressures are known, only the pressure distribution is required for the computation of the effective area. In the approach by Dadson [25] the pressure distribution, which depends only on the gap geometry and the inlet and outlet pressures, is given in a closed form expression in Eq. (2.3.3). The involved integrals are computed by implementing the numerical integration scheme presented in Appendix A. When the flow inside the PCA gap is simulated with Fluent the pressure distribution, which is part of the converged solution, can be exported along the gap in a data file and all numerical operations required to compute the piston effective area are performed on the extracted pressure values. In the kinetic approach implementation for the computation of the pressure distribution an iterative procedure is required. The work of [40] is used in order to create a robust kinetic database of the dimensionless mass flow rate with respect to 76 values for

the rarefaction parameter and 21 values for the radius ratio. The dimensionless flow rate against gas rarefaction is presented in Fig. 6 for various radius ratios.

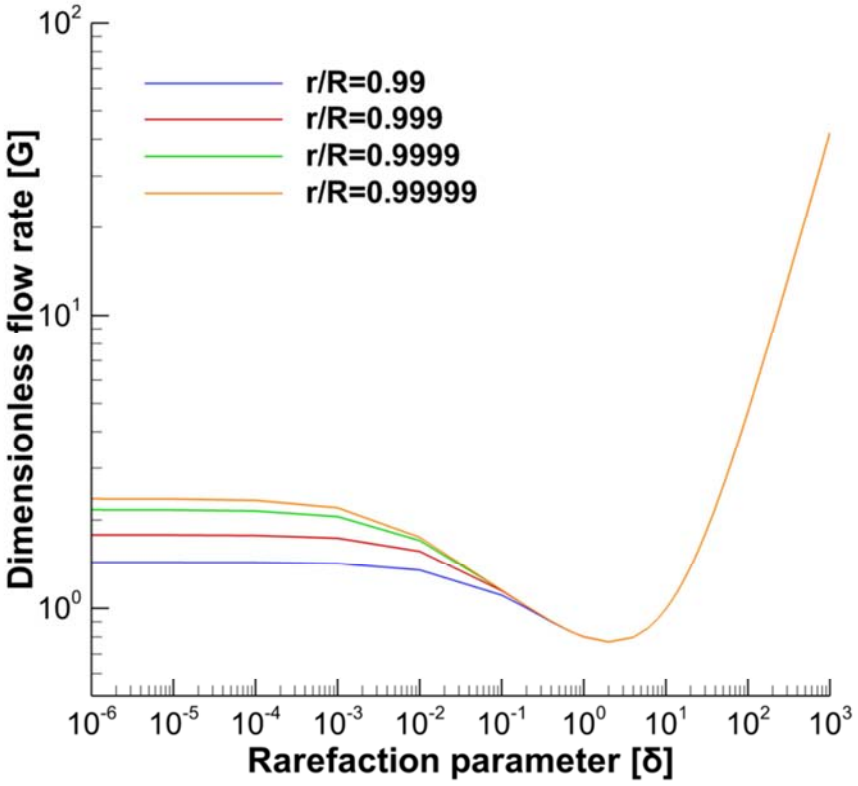

Figure 6: Dimensionless flow rate G against gas rarefaction for various radius ratios.

Starting from the gap inlet and assuming an initial value for the mass flow rate Eq. 2.3.13 can be solved explicitly by applying the forward Euler method in order to determine the pressure distribution along the gap. The assumption of the mass flow rate is based on the bisection method where the selected interval is [0, 1]. The procedure is iterated upon convergence for the outlet pressure. All the described approaches to simulate the gas flow inside a piston cylinder gap and calculate the effective area have been integrated in an in-house Fortran code.

3.3 Benchmark

To verify all the approaches implemented in the code two PCA gaps will be simulated. In the first case the gap has a linear width profile while in the second case the gap width profile is polynomial. The dimensional and operational data of the two cases are presented in Table 2.

Table 2: Dimensional and operational data for the linear and polynomial gap benchmark cases.

PCA data	Linear gap case	Polynomial gap case
L [m]	0.05	0.05
r_o [m]	0.02	0.02
r [m]	$0.02+4\cdot10^{-4}z$	$0.02+8\cdot10^{-4}z-8\cdot10^{-3}z^2$
R [m]	$0.02005-2\cdot10^{-4}z$	$0.02005-1\cdot10^{-3}z+1.6\cdot10^{-2}z^2$
P_{in} [Pa]	150000	150000
P_{out} [Pa]	$[10,100000]$	$[10,100000]$

The effective area is calculated for both the approximate and exact approaches while the benchmark simulations involve:

- The Dadson theory approach implemented in Mathematica.
- The Dadson theory approach implemented in Fortran.
- The CFD approach where the Fortran code only computes the effective area based on the pressure distribution provided by Fluent.
- The kinetic approach implemented in Fortran.

The benchmark results for the linear gap case are presented in Table 3. Since the results for the effective area require a high accuracy, the relative deviations between the different approaches are multiplied by 10^6 and thus are given in ppm. The comparison between the Mathematica and Fortran implementation of Dadson theory has a perfect agreement with a highest relative deviation of 0.23 ppm in the exact approach. In addition, the results between the Dadson and the CFD approach show a good agreement with the highest deviation of 0.66 ppm appearing in the approximate approach. Finally, as expected kinetic theory shows a good agreement with Dadson and CFD results for high outlet pressures with a deviation of 0.52 ppm and 0.48 ppm at 100 kPa respectively. While as the outlet pressure decreases the discrepancies between viscous and kinetic results increase reaching a relative deviation of 1.50 ppm with Dadson and 2.16 ppm with CFD results.

Table 3: Effective area of the linear gap benchmark case in cm^2 case computed with the approximate and exact approaches.

Approximate approach				
Outlet Pressure [Pa]	Dadson Theory (Mathematica)	Dadson Theory (Fortran)	CFD (Fluent-Fortran)	Kinetic Theory (Fortran)
100000	12.6024372	12.6024372	12.6024367	12.6024307
50000	12.6026542	12.6026542	12.6026555	12.6026433
10000	12.6028892	12.6028892	12.6028975	12.6028717
5000	12.6029240	12.6029240	12.6029340	12.6029052
1000	12.6029528	12.6029522	12.6029607	12.6029328
100	12.6029595	12.6029581	12.6029665	12.6029391
10	12.6029601	12.6029587	12.6029670	12.6029397
Exact approach				
Outlet Pressure [Pa]	Dadson Theory (Mathematica)	Dadson Theory (Fortran)	CFD (Fluent-Fortran)	Kinetic Theory (Fortran)
100000	12.6024567	12.6024567	12.6024560	12.6024501
50000	12.6026744	12.6026744	12.6026757	12.6026634
10000	12.6029103	12.6029103	12.6029184	12.6028927
5000	12.6029452	12.6029451	12.6029548	12.6029263
1000	12.6029741	12.6029729	12.6029788	12.6029540
100	12.6029808	12.6029781	12.6029837	12.6029603
10	12.6029815	12.6029785	12.6029842	12.6029610

The benchmark results for the polynomial gap case are presented in Table 4. In this case the results provided by the Mathematica and Fortran implementation of Dadson theory also have a perfect agreement with a highest relative deviation of 0.13 ppm in the exact approach. Furthermore, the comparison of Dadson results against the CFD ones shows a great agreement with a highest relative deviation of 0.30 ppm in the approximate approach. In the polynomial gap case the gap is narrower than the linear case and thus the discrepancies between the kinetic and viscous theories are higher. For an outlet pressure of 100000 Pa the relative deviation between kinetic and Dadson results is 0.54 ppm and increases to 3.98 ppm at 10 Pa. The respective deviation between kinetic and CFD results are 0.50 ppm and 4.28 ppm.

Table 4: Effective area of the polynomial gap benchmark case in cm^2 case computed with the approximate and exact approaches.

Approximate approach				
Outlet Pressure [Pa]	Dadson Theory (Mathematica)	Dadson Theory (Fortran)	CFD (Fluent-Fortran)	Kinetic Theory (Fortran)
100000	12.6024372	12.6024372	12.6024367	12.6024307
50000	12.6026542	12.6026542	12.6026555	12.6026433
10000	12.6028892	12.6028892	12.6028975	12.6028717
5000	12.6029240	12.6029240	12.6029340	12.6029052
1000	12.6029528	12.6029522	12.6029607	12.6029328
100	12.6029595	12.6029581	12.6029665	12.6029391
10	12.6029601	12.6029587	12.6029670	12.6029397
Exact approach				
Outlet Pressure [Pa]	Dadson Theory (Mathematica)	Dadson Theory (Fortran)	CFD (Fluent-Fortran)	Kinetic Theory (Fortran)
100000	12.6024567	12.6024567	12.6024560	12.6024501
50000	12.6026744	12.6026744	12.6026757	12.6026634
10000	12.6029103	12.6029103	12.6029184	12.6028927
5000	12.6029452	12.6029451	12.6029548	12.6029263
1000	12.6029741	12.6029729	12.6029788	12.6029540
100	12.6029808	12.6029781	12.6029837	12.6029603
10	12.6029815	12.6029785	12.6029842	12.6029610

Chapter 4: Simulation of the FPG8601 and FRS4 piston gauges

4.1 Fixed Pressure Gauge: FPG8601

4.1.1 Dimensional and operational data

As described in Chapter 2 in the FPG8601 the lubricating gas flow enters the piston-cylinder gap radially from the middle section of the cylinder and flows through the gap towards the two pressure chambers located at the PCA extremities. In order to simulate the gas flow the gap is divided into two parts as shown in Fig. 7. The upper part connects the gas inlet with the measurement pressure chamber, while the lower part connects the gas inlet to the reference pressure chamber. The two parts are simulated in both gauge and absolute operation modes and their respective effective areas are computed separately.

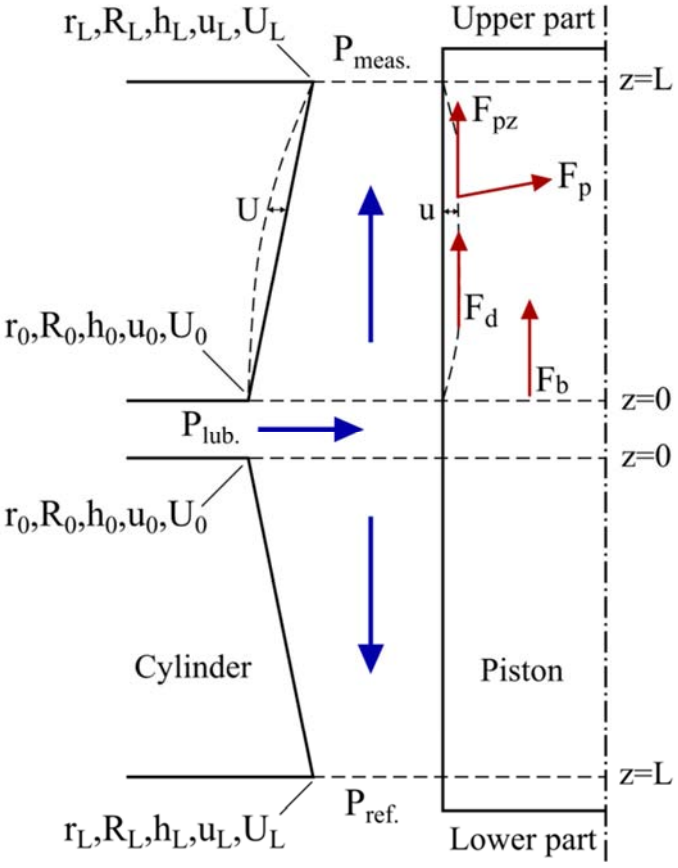

Figure 7: Representation of an FPG gap cross section simulation.

The outlet pressure of the upper part corresponds to the measurement pressure and for the simulations it ranges from 100001 Pa to 115000 Pa in gauge mode and from 1 Pa up to 15000 Pa in absolute mode. The outlet pressure of the lower part corresponds to the reference pressure and for the simulations it ranges from 100001 Pa to 100010 Pa in gauge mode and from 1 Pa to 10 Pa in absolute mode. The inlet pressure in either the upper or lower part corresponds to the lubrication pressure and is set 40 kPa higher than the reference pressure in both gauge and absolute operation modes. Finally, the simulating gas is assumed to be dry N_2 at 20 ^{o}C.

In the frame of the second work package of the EMPIR 14IND06 pres2vac project three FPG8601 gauges have been dimensionally characterized by PTB (Physikalisch-Technische Bundesanstalt), SP (Swedish National Testing Institute) and INRIM (Istituto Nazionale di Ricerca Metrologica). The complete dimensional analysis, which included the straightness and roundness data, has been delivered to UTH in order to simulate the gas flow inside the piston-cylinder gap. In Table 5 the measurement characteristics for each of the three FPGs are presented. The piston and cylinder radii measurements used in the FPG simulations averaged over all angles are presented in Fig. 8. The piston radius profile of the SP and INRIM FPGs are quite similar in both the upper and lower parts. In addition, their cylinder profiles are close aside from the narrowing existing in the lower part exit of SP's gauge. The FPG characterized by PTB has a larger piston radius leading to a larger piston area and a wider gap exit leading to lower gas rarefaction.

Table 5: Measurement and dimensional characteristics of FPG assemblies provided by PTB, SP and INRIM.

FPG device	PTB	SP	INRIM	PTB	SP	INRIM
FPG Part		Upper			Lower	
Measurement angles	8	8	4	8	8	4
Angle interval [deg]	45	45	45	45	45	45
Measurements	343	317	69	339	346	69
Measurement interval [mm]	0.1	0.1	0.5	0.1	0.1	0.5
Engagement length [mm]	34.2	31.6	34.0	33.8	34.5	34.0
Average piston radius [mm]	17.66640	17.66581	17.66583	17.66638	17.66583	17.66582
Average cylinder radius [mm]	17.66891	17.66843	17.66830	17.66893	17.66832	17.66830
Average gap inlet [μm]	4.646	3.889	4.238	4.414	3.784	4.131
Average gap width [μm]	2.511	2.617	2.474	2.551	2.490	2.486
Average gap outlet [μm]	2.013	1.015	1.087	2.155	1.553	0.922
Average piston area [cm^2]	9.804960	9.804314	9.804328	9.804938	9.804326	9.804315

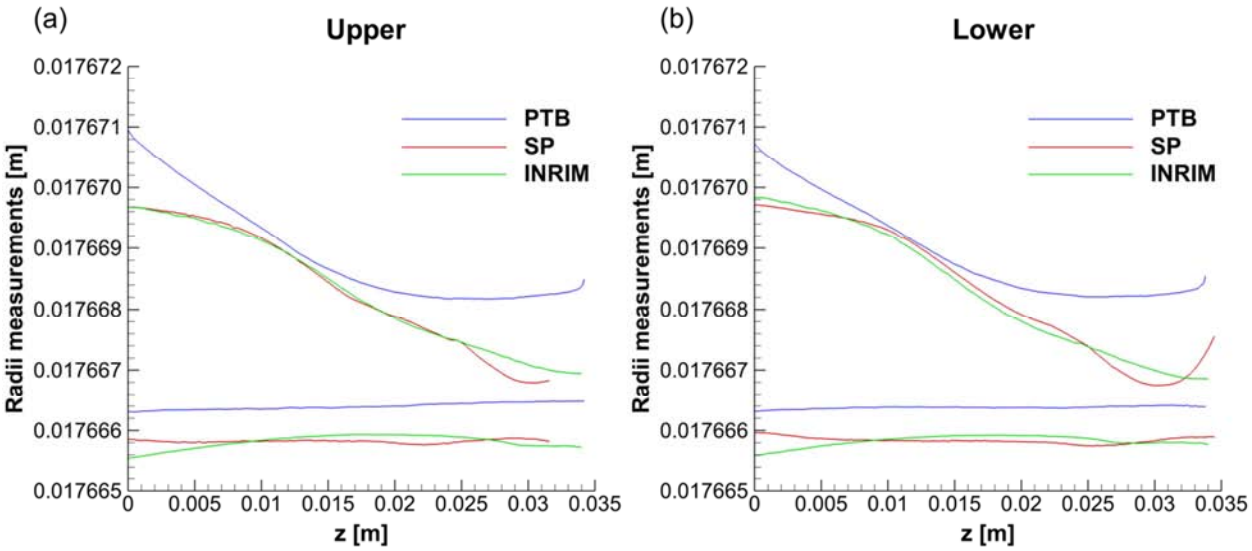

Figure 8: Piston and cylinder radii measurements provided by PTB, SP and INRIM averaged over all angles for (a) the upper part; (b) the lower part.

4.1.2 Effective area: approximate approach

Simulations have been performed to calculate the effective area of the three piston cylinder assemblies dimensionally characterized by PTB, SP and INRIM based on the approximate approach. In Fig. 9 the effective area results for the FPG assembly of PTB based on Dadson theory, Fluent and kinetic theory are provided. In addition, computations performed by PTB based on Dasdon and kinetic theories for their FPG configuration are also included in Fig. 9 for comparison purposes. In order to have a uniform representation for the effective areas in the gauge and absolute operation modes all FPG results are presented with respect to $P - P_{op}$ where P is the outlet pressure of the gap part under investigation, while P_{op} is set to 100 kPa in gauge mode and 0 Pa in absolute mode. The piston effective areas computed based on Dadson theory by UTH and PTB show a satisfactory agreement in both FPG parts and operation modes. The highest relative deviations appear in the absolute mode and are 2.95 ppm and 1.23 ppm for the upper and lower part respectively. The kinetic results provided by UTH and PTB show a good agreement with a constant relative deviation of 0.25 ppm for the upper part and about 1.1 ppm for the lower part. Comparisons between Dadson theory and Fluent results show very good agreement in all simulations performed with a highest relative deviation of 0.56 ppm. Furthermore, it is clear that viscous results will deviate from kinetic ones as gas rarefaction is

increased. In Fig. 9, Dadson results show discrepancies with respect to kinetic theory below 0.72 ppm in gauge mode and up to 2.46 ppm in absolute mode for both FPG parts. In Table 6 the effect of the gas flow and piston variation on the effective area based on kinetic theory is provided. It is observed that, the ratio of the effective area due to the gas flow and variation of the piston radius over the effective area is constant in the lower part with an average of 124.8 ppm while it slightly deviates from an average of 124.1 ppm in the upper part of the FPG.

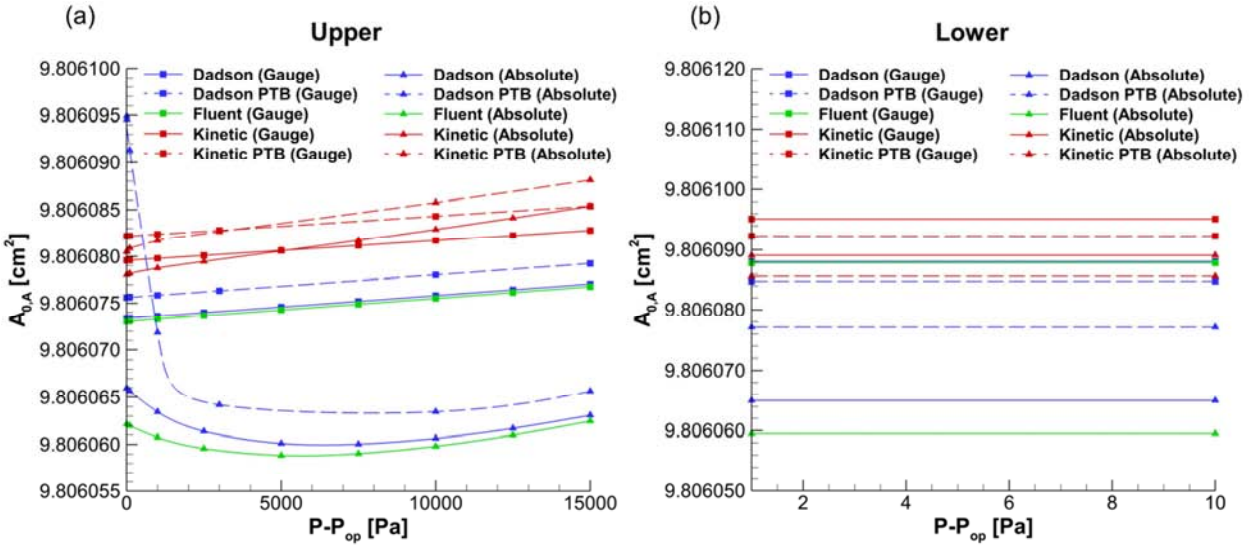

Figure 9: Effective area calculations for the FPG assembly of PTB based on the approximate approach for the (a) upper part; (b) lower part.

Table 6: Effect of gas flow and piston radius variation on the effective area for the FPG assembly of PTB based on the approximate approach.

Operation mode		Gauge			Absolute		
FPG Part	$P - P_{op}$ [Pa]	$A_{0,A}$ [cm^2]	$A_{2,A}$ [cm^2]	$\frac{A_{2,A}}{A_{0,A}} \cdot 10^6$	$A_{0,A}$ [cm^2]	$A_{2,A}$ [cm^2]	$\frac{A_{2,A}}{A_{0,A}} \cdot 10^6$
Upper	1	9.806080	0.001216	124.0	9.806080	0.001216	124.0
	100	9.806080	0.001216	124.0	9.806080	0.001216	124.0
	1000	9.806080	0.001216	124.0	9.806080	0.001216	124.0
	5000	9.806080	0.001217	124.1	9.806080	0.001217	124.1
	10000	9.806081	0.001218	124.2	9.806081	0.001218	124.2
	15000	9.806083	0.001219	124.3	9.806083	0.001219	124.3
Lower	1	9.806095	0.001227	125.1	9.806095	0.001227	125.1
	10	9.806095	0.001227	125.1	9.806095	0.001227	125.1

In Fig. 10 the effective area computations performed based on Dadson theory, Fluent and kinetic theory are presented for the FPG configuration of SP. As shown above for the FPG configuration of PTB, Dadson and Fluent results also show a great agreement in all simulations performed for the SP configuration. The relative deviations between the two approaches are below 0.20 ppm and 0.07 ppm for the upper and lower parts respectively. In this configuration Dadson and kinetic results show relative deviations below 2.85 ppm and 2.26 ppm in the upper and lower parts for the gauge mode. However, the above discrepancies are increased when the gauge is operated under absolute pressure conditions to a highest value of 13.36 for the upper part and 3.02 ppm for the lower part.

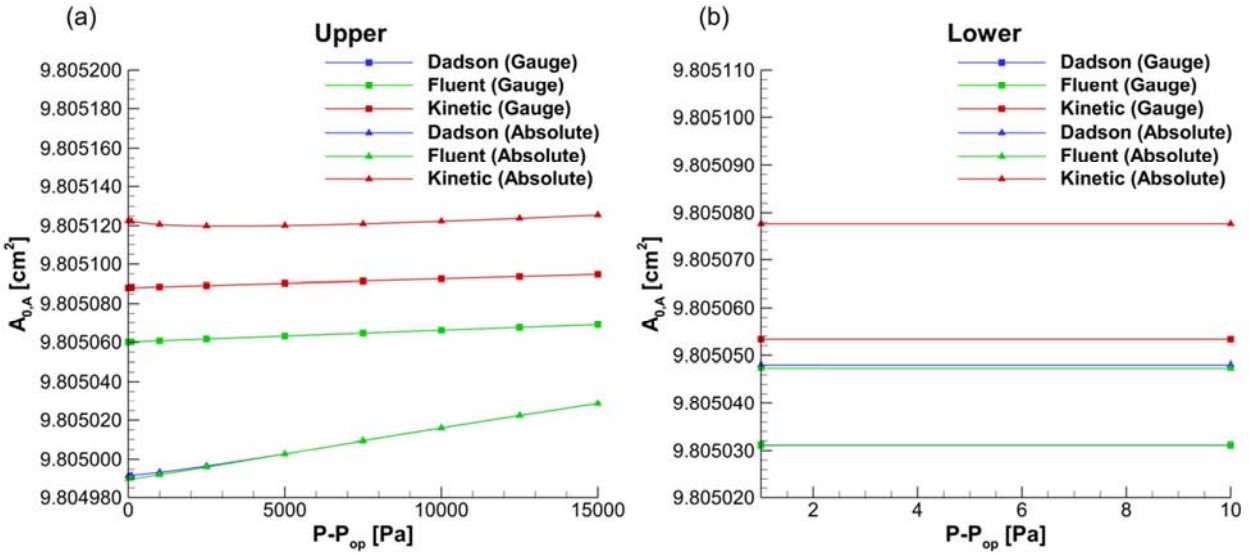

Figure 10: Effective area calculations for the FPG assembly of SP based on the approximate approach for the (a) upper part; (b) lower part.

In the upper part a deviation between viscous and kinetic results of the order of 10 ppm is justified since the gap outlet in this configuration is narrower than that of PTB. While, in the lower part the gap outlet width is closer to the outlet of PTB. Thus, the gas is less rarefied as it exits the gap justifying the smaller deviations between viscous and kinetic results. Tabulated kinetic results for the effect of the gas flow and piston variation on the effective area are provided in Table 7. The gas flow has a weaker effect on the piston effective area of the SP FPG configuration. In the lower part the ratio of the effective area due to the gas flow and piston variation over the piston effective area is 59.8 ppm and 62.3 ppm in the gauge and absolute mode

respectively. While in the upper part it deviates slightly around 74.8 ppm when the FPG is operated under gauge mode and around 78.0 ppm under absolute mode.

Table 7: Effect of gas flow and piston radius variation on the effective area for the FPG assembly of SP based on the approximate approach.

Operation mode		Gauge			Absolute		
FPG Part	$P - P_{op}$ [Pa]	$A_{0,A}$ [cm^2]	$A_{2,A}$ [cm^2]	$\frac{A_{2,A}}{A_{0,A}} \cdot 10^6$	$A_{0,A}$ [cm^2]	$A_{2,A}$ [cm^2]	$\frac{A_{2,A}}{A_{0,A}} \cdot 10^6$
Upper	1	9.805088	0.000730	74.55	9.805122	0.000765	78.06
	100	9.805088	0.000731	74.56	9.805122	0.000765	78.03
	1000	9.805088	0.000731	74.60	9.805121	0.000764	77.87
	5000	9.805090	0.000733	74.78	9.805120	0.000763	77.82
	10000	9.805093	0.000735	75.01	9.805122	0.000765	78.05
	15000	9.805095	0.000738	75.23	9.805126	0.000768	78.37
Lower	1	9.805053	0.000586	59.78	9.805078	0.000611	62.26
	10	9.805053	0.000586	59.78	9.805078	0.000611	62.26

In Fig. 11 the effective area for the FPG of INRIM computed based on Dadson theory, Fluent and kinetic theory are presented. Alongside the FPG configurations of PTB and SP, Dadson and Fluent approaches provide results with good agreement in all simulations performed for the FPG device of INRIM. The two viscous approaches have relative deviations below 0.35 ppm and 0.41 ppm in the upper and lower parts respectively. In Fig. 11 Dadson and kinetic results show relative deviations below 1.97 ppm and 2.22 ppm in the upper and lower part under gauge operation. However, the above deviations are increased under absolute mode operation to a highest value of 12.99 ppm for the upper and 12.22 ppm for the lower PCA part. In Table 8 the kinetic results for the effect of the gas flow and piston radius variation on the piston effective area are provided for the FPG of INRIM. The gas flow in this configuration has a similar effect on the piston effective area with PTB's configuration. In the lower part, the ratio of the effective area due to the gas flow over the piston effective area is 108.6 ppm and 110.3 in gauge and absolute mode. In addition, for the upper part it deviates slightly around an average of 121.4 ppm and 122.3 ppm under gauge and absolute mode respectively.

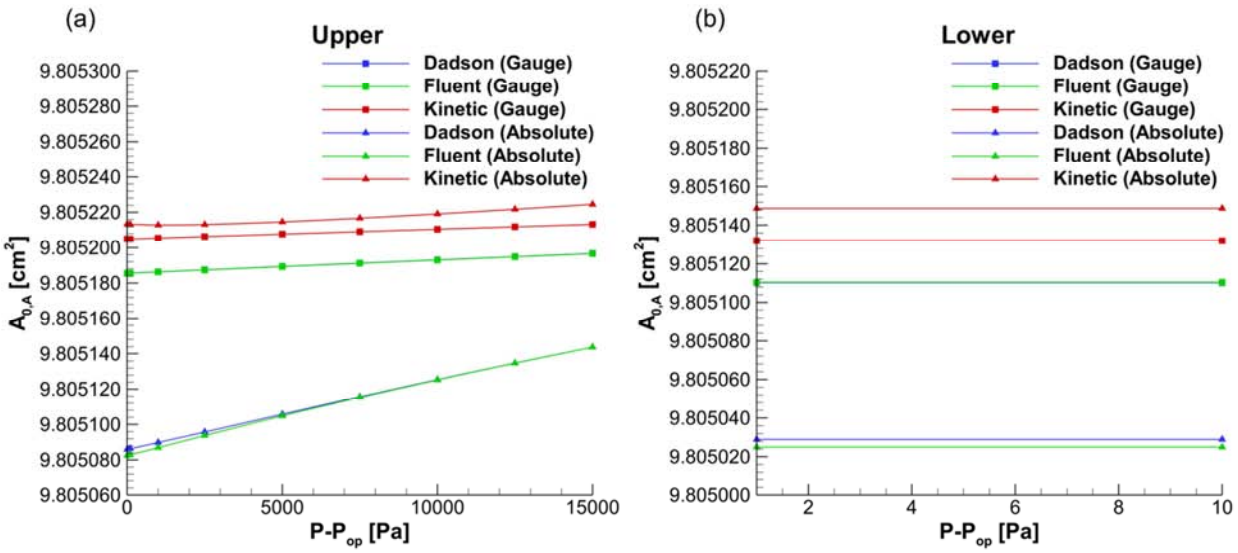

Figure 11: Effective area calculations for the FPG assembly of INRIM based on the approximate approach for the (a) upper part; (b) lower part.

Table 8: Effect of gas flow and piston radius variation on the effective area for the FPG assembly of INRIM based on the approximate approach.

Operation mode		Gauge			Absolute		
FPG Part	$P - P_{op}$ [Pa]	$A_{0,A}$ [cm^2]	$A_{2,A}$ [cm^2]	$\frac{A_{2,A}}{A_{0,A}} \cdot 10^6$	$A_{0,A}$ [cm^2]	$A_{2,A}$ [cm^2]	$\frac{A_{2,A}}{A_{0,A}} \cdot 10^6$
Upper	1	9.805205	0.001187	121.1	9.805213	0.001196	122.0
	100	9.805205	0.001188	121.1	9.805213	0.001196	122.0
	1000	9.805205	0.001188	121.2	9.805213	0.001195	121.9
	5000	9.805208	0.001190	121.4	9.805215	0.001197	122.1
	10000	9.805210	0.001193	121.7	9.805219	0.001202	122.6
	15000	9.805213	0.001196	122.0	9.805225	0.001207	123.1
Lower	1	9.805132	0.001065	108.6	9.805149	0.001082	110.3
	10	9.805132	0.001065	108.6	9.805149	0.001082	110.3

4.1.3 Effective area: exact approach

Simulations have been performed to compute the effective area of the three FPG configurations that have been dimensionally characterized by PTB, SP and INRIM based on the exact approach. In Fig. 12 results for the effective area of the FPG characterized by PTB based on Dadson theory, Fluent and kinetic theory are shown. As in the approximate approach the agreement between Dadson and Fluent results based on the exact approach is good in all simulations with the highest relative deviation reaching 0.44 ppm. In addition, Dadson results

show relative discrepancies with respect to kinetic ones below 0.72 ppm in gauge mode and up to 2.62 ppm in absolute mode for both FPG parts. As mentioned above, it is also noted here that the FPG configuration of PTB has a slightly larger piston which leads to an overall larger effective area and a wider gap exit leading to lower gas rarefaction. Thus, discrepancies of a couple parts per million between viscous and kinetic results in the absolute mode are justified.

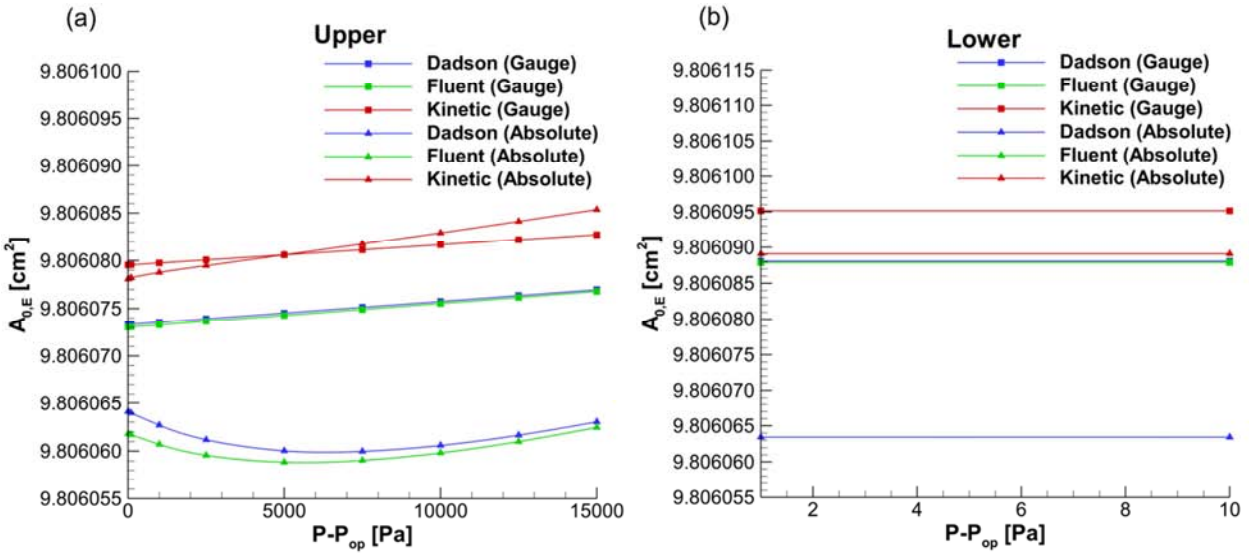

Figure 12: Effective area calculations for the FPG assembly of PTB based on the exact approach for the (a) upper part; (b) lower part.

Tabulated results for the effect of the gas flow on the effective area based on kinetic theory for the FPG configuration of PTB are provided in Table 9. The ratio of the effective area due to the drag force exerted on the piston over the overall piston effective area is 116.2 ppm in the lower part, while it deviates around an average of 110.1 ppm in the upper part. As expected, the effect of the normal component of the pressure force on the overall effective is higher under gauge conditions due to the higher operating pressures inside the piston-cylinder clearance. In Table 9 it is shown that the ratio of the effective area due to the normal component of the pressure force over the overall effective area reaches a highest value of 102.2 ppm in gauge mode and 25.5 ppm in absolute mode.

Table 9: Effect of gas flow on the effective area for the FPG assembly of PTB based on the exact approach.

Gauge operation mode						
FPG Part	$P - P_{ref}$ [Pa]	$A_{0,E}$ [cm^2]	$A_{2,E}$ [cm^2]	$A_{3,E}$ [cm^2]	$\frac{A_{2,E}}{A_{0,E}} \cdot 10^6$	$\frac{A_{3,E}}{A_{0,E}} \cdot 10^6$
Upper	1	9.806080	0.001079	0.00061	110.0	62.00
	100	9.806080	0.001079	0.00061	110.0	62.17
	1000	9.806080	0.001079	0.00062	110.1	63.71
	5000	9.806081	0.001080	0.00070	110.2	71.56
	10000	9.806082	0.001082	0.00083	110.3	84.32
	15000	9.806083	0.001083	0.00100	110.5	102.2
Lower	1	9.806095	0.001143	0.00030	116.5	30.31
	10	9.806095	0.001143	0.00030	116.5	30.31
Absolute operation mode						
FPG Part	$P - P_{ref}$ [Pa]	$A_{0,E}$ [cm^2]	$A_{2,E}$ [cm^2]	$A_{3,E}$ [cm^2]	$\frac{A_{2,E}}{A_{0,E}} \cdot 10^6$	$\frac{A_{3,E}}{A_{0,E}} \cdot 10^6$
Upper	1	9.806078	0.001075	0.000139	109.7	14.19
	100	9.806078	0.001075	0.000140	109.7	14.25
	1000	9.806079	0.001076	0.000144	109.7	14.71
	5000	9.806081	0.001078	0.000166	109.9	16.91
	10000	9.806083	0.001081	0.000201	110.3	20.47
	15000	9.806085	0.001085	0.000250	110.6	25.48
Lower	1	9.806089	0.001136	0.000085	115.9	8.620
	10	9.806089	0.001136	0.000085	115.9	8.620

The effective area calculations based on Dadson theory, Fluent and kinetic theory for the FPG device of SP are presented in Fig. 13. The comparison between the two viscous approaches shows an excellent agreement with a highest relative deviation of 0.33 ppm. In this configuration Dadson and kinetic results show relative deviations below 2.85 ppm in gauge mode. As expected, in absolute mode the above deviations are increased to a peak value of 13.71 ppm and 2.85 ppm for the upper and lower FPG parts. In Table 10 the effect of the gas flow on the effective area based on kinetic theory is provided. The ratio of the effective area due to the drag force over the overall piston effective area is 73.5 ppm in the lower part, while in the upper part it deviates around an average of 80.4 ppm in absolute mode and in 76.9 gauge mode. In addition, the effect of the normal component of the pressure force on the effective area reaches 28.2 ppm and 12.6 ppm in gauge and absolute modes respectively.

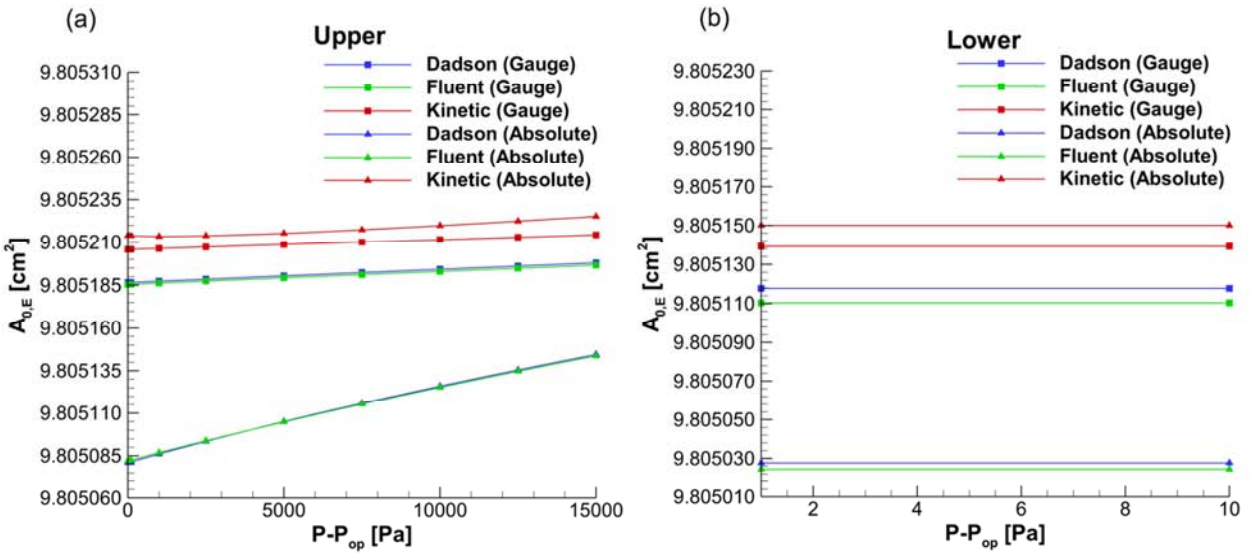

Figure 13: Effective area calculations for the FPG assembly of SP based on the exact approach for the (a) upper part; (b) lower part.

Table 10: Effect of gas flow on the effective area for the FPG assembly of SP based on the exact approach.

Gauge operation mode						
FPG Part	$P-P_{ref}$ [Pa]	$A_{0,E}$ [cm^2]	$A_{2,E}$ [cm^2]	$A_{3,E}$ [cm^2]	$\frac{A_{2,E}}{A_{0,E}}\cdot 10^6$	$\frac{A_{3,E}}{A_{0,E}}\cdot 10^6$
Upper	1	9.805086	0.000752	-0.000124	76.67	-12.62
	100	9.805086	0.000752	-0.000124	76.67	-12.66
	1000	9.805087	0.000752	-0.000127	76.72	-13.00
	5000	9.805088	0.000754	-0.000145	76.91	-14.74
	10000	9.805090	0.000757	-0.000172	77.15	-17.55
	15000	9.805092	0.000759	-0.000211	77.39	-21.49
Lower	1	9.805054	0.000708	-0.000276	72.17	-28.19
	10	9.805054	0.000708	-0.000276	72.17	-28.19
Absolute operation mode						
FPG Part	$P-P_{ref}$ [Pa]	$A_{0,E}$ [cm^2]	$A_{2,E}$ [cm^2]	$A_{3,E}$ [cm^2]	$\frac{A_{2,E}}{A_{0,E}}\cdot 10^6$	$\frac{A_{3,E}}{A_{0,E}}\cdot 10^6$
Upper	1	9.805122	0.000789	-0.000023	80.43	-2.380
	100	9.805122	0.000789	-0.000023	80.40	-2.390
	1000	9.805120	0.000787	-0.000024	80.25	-2.490
	5000	9.805120	0.000786	-0.000029	80.20	-3.000
	10000	9.805122	0.000789	-0.000037	80.45	-3.820
	15000	9.805125	0.000792	-0.000049	80.80	-4.960
Lower	1	9.805078	0.000734	-0.000124	74.87	-12.60
	10	9.805078	0.0007340	-0.000124	74.87	-12.60

In Fig. 14 the effective area results for the FPG configuration of INRIM computed based on Dadson theory, Fluent and kinetic theory are presented. Alongside the FPG configurations of PTB and SP, Dadson and Fluent approaches provide results with good agreement in all simulations performed for the FPG device of INRIM. The two viscous approaches have relative deviations below 0.33 in the upper ppm and 0.75 ppm in the lower gap part. In this configuration Dadson and kinetic results show relative deviations below 1.96 ppm and 2.18 ppm in the upper and lower parts under gauge operation. However, the above deviations increase under absolute mode operation of the FPG with a highest value of 13.6 and 12.5 for the upper and lower gap parts. Kinetic results for the effect of the gas flow on the effective area are provided in Table 11. The effective area due to the drag force and the overall effective area have a ratio of 82.4 ppm in the lower part, while in the upper part this ratio deviates around an average of 91.0 ppm. In addition, the ratio of the effective area due to the normal component of the pressure force on the effective area has a highest value of 123.6 ppm in gauge mode and 43.1 ppm in absolute mode.

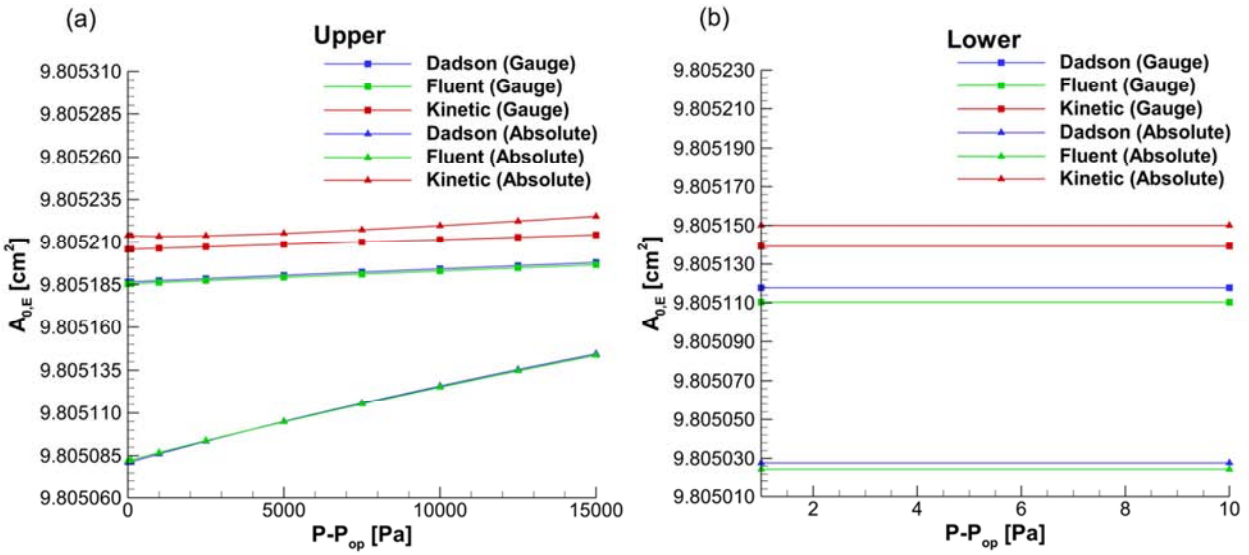

Figure 14: Effective area calculations for the FPG assembly of INRIM based on the exact approach for the (a) upper part; (b) lower part.

Table 11: Effect of gas flow on the effective area for the FPG assembly of INRIM based on the exact approach.

Gauge operation mode						
FPG Part	$P - P_{ref}$ [Pa]	$A_{0,E}$ [cm^2]	$A_{2,E}$ [cm^2]	$A_{3,E}$ [cm^2]	$\frac{A_{2,E}}{A_{0,E}} \cdot 10^6$	$\frac{A_{3,E}}{A_{0,E}} \cdot 10^6$
Upper	1	9.805206	0.000886	0.000796	90.31	81.18
	100	9.805206	0.000886	0.000798	90.31	81.35
	1000	9.805206	0.000886	0.000814	90.35	83.00
	5000	9.805209	0.000888	0.000895	90.53	91.31
	10000	9.805211	0.000890	0.001027	90.74	104.8
	15000	9.805211	0.000892	0.001212	90.96	123.6
Lower	1	9.805139	0.000800	0.000768	81.61	78.35
	10	9.805139	0.000800	0.000768	81.61	78.35
Absolute operation mode						
FPG Part	$P - P_{ref}$ [Pa]	$A_{0,E}$ [cm^2]	$A_{2,E}$ [cm^2]	$A_{3,E}$ [cm^2]	$\frac{A_{2,E}}{A_{0,E}} \cdot 10^6$	$\frac{A_{3,E}}{A_{0,E}} \cdot 10^6$
Upper	1	9.805214	0.000894	0.000302	91.18	30.84
	100	9.805214	0.000894	0.000303	91.18	30.89
	1000	9.805213	0.000894	0.000307	91.16	31.33
	5000	9.805215	0.000895	0.000330	91.31	33.72
	10000	9.805220	0.000899	0.000369	91.68	37.65
	15000	9.805225	0.000903	0.000423	92.10	43.14
Lower	1	9.805150	0.000816	0.000267	83.25	27.21
	10	9.805150	0.000816	0.000267	83.25	27.21

4.1.4 Effective area: effect of measurements

The effective areas for the FPG configurations of PTB, SP and INRIM computed by the approximate and the exact approaches have been presented above. The results for the effective area averaged over all angles based on the two approaches show a highest relative deviation of 0.75 ppm. Moreover, in specific cross sections these deviations reach up to 2.75 ppm. These deviations originate either from the approximations introduced in Eq. 3.1.9 or from numerical error in the derivative of the piston radius in Eq. 3.1.2. In order to have a proper comparison between the two approaches the three FPG configurations were simulated based on polynomial least squares approximations of the piston and cylinder radii. The least squares expressions were derived from the real dimensional data provided by PTB, SP and INRIM for all angles. In addition, to achieve an adequate approximation of the real geometry least squares

approximations were derived iteratively, by increasing the degree of the interpolating polynomial upon convergence of the widely known statistical coefficient R^2. In Fig. 15 the piston and cylinder radii measurements and the corresponding least squares approximations averaged over all angles are presented for the three FPG assemblies. It is observed that the least squares polynomials adequately represent the real geometry of the PCAs, while omitting the piston radius variation originating from the surface roughness and the uncertainties of the performed dimensional measurements.

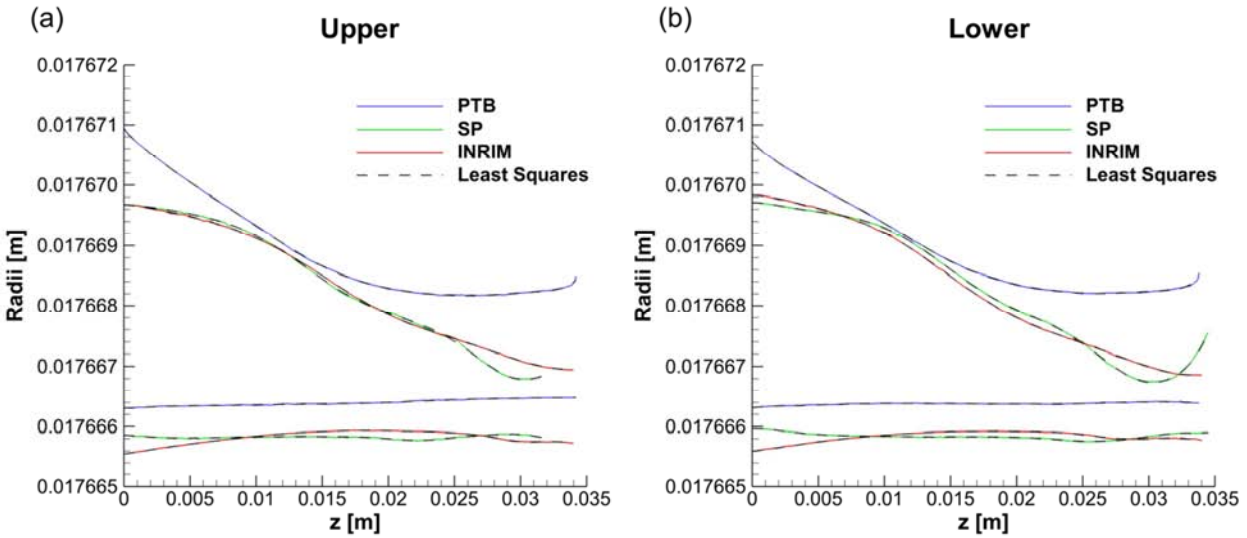

Figure 15: Piston and cylinder radii measurements of FPG assemblies provided by PTB, SP and INRIM and corresponding least squares approximations averaged over all angles for (a) the upper part; (b) the lower part.

In Table 12 the kinetic results for the effective areas computed by the approximate and exact approaches based on the least squares polynomials are presented for the three FPG configurations. For the PTB and SP configuration the average relative deviations between the two approaches are decreased to a highest value of $8 \cdot 10^{-4}$ ppm and $5 \cdot 10^{-4}$ ppm respectively. While for the configuration of INRIM the highest relative deviation reaches a peak value of $1.8 \cdot 10^{-3}$. In addition, it is observed that when the kinetic simulations are performed on the interpolated radii the deviations are decreased by a factor of around 100 on average. Thus, it is noted that the deviations between the two approaches are originating from the numerical error introduced in the derivative of the piston radius required for the computation of the exact

approach. It is also worthwhile to mention that increasing the order of the differentiating scheme will not lead to better agreement between the two approaches.

Table 12: Effective area computed by the approximate and exact approaches based on polynomial least squares approximations for the FPG assemblies of PTB, SP and INRIM.

Operation Mode		Gauge					
FPG configuration		PTB		SP		INRIM	
FPG Part	$P - P_{op}$ [Pa]	$A_{0,A}$ [cm^2]	$A_{0,E}$ [cm^2]	$A_{0,A}$ [cm^2]	$A_{0,E}$ [cm^2]	$A_{0,A}$ [cm^2]	$A_{0,E}$ [cm^2]
Upper	1	9.8060800	9.8060800	9.8050878	9.8050878	9.8052062	9.8052063
	100	9.8060800	9.8060800	9.8050878	9.8050878	9.8052063	9.8052063
	1000	9.8060802	9.8060802	9.8050882	9.8050882	9.8052068	9.8052068
	5000	9.8060811	9.8060811	9.8050901	9.8050901	9.8052092	9.8052092
	10000	9.8060822	9.8060822	9.8050923	9.8050923	9.8052120	9.8052120
	15000	9.8060832	9.8060832	9.8050945	9.8050945	9.8052148	9.8052148
Lower	1	9.8060895	9.8060895	9.8050522	9.8050522	9.8051327	9.8051327
	10	9.8060895	9.8060895	9.8050522	9.8050522	9.8051327	9.8051327
Operation Mode		Absolute					
FPG configuration		PTB		SP		INRIM	
FPG Part	$P - P_{op}$ [Pa]	$A_{0,A}$ [cm^2]	$A_{0,E}$ [cm^2]	$A_{0,A}$ [cm^2]	$A_{0,E}$ [cm^2]	$A_{0,A}$ [cm^2]	$A_{0,E}$ [cm^2]
Upper	1	9.8060783	9.8060783	9.80512399	9.80512399	9.8052188	9.8052188
	100	9.8060785	9.8060785	9.8051233	9.8051233	9.8052180	9.8052180
	1000	9.8060791	9.8060791	9.8051209	9.8051209	9.8052156	9.8052156
	5000	9.8060809	9.8060809	9.8051199	9.8051199	9.8052160	9.8052160
	10000	9.8060833	9.8060833	9.8051221	9.8051221	9.8052203	9.8052203
	15000	9.8060858	9.8060858	9.8051253	9.8051253	9.8052258	9.8052258
Lower	1	9.8060895	9.8060895	9.8050767	9.8050767	9.8051536	9.8051537
	10	9.8060895	9.8060895	9.8050767	9.8050767	9.8051536	9.8051537

4.1.5 Effective area: whole PCA

In order to calculate the effective area of the whole PCA all the forces acting on the piston must be taken into account:

$$A_{total} = \frac{F_L - F_U - F_0}{P_{meas} - P_{ref}} \tag{4.1.1}$$

where F_L and F_U are the forces acting on the lower and upper parts of the PCA respectively, while F_0 is the remaining force acting on the piston from the load cell zeroing. Substituting the forces with the corresponding expressions for the effective areas the total effective area of the FPG can be written as:

$$A_{total} = \frac{(P_{lub} - P_{ref})A_L - (P_{lub} - P_{meas})A_U}{P_{meas} - P_{ref}} - \frac{(P_{lub,0} - P_{ref,0})A_{L,0} - (P_{lub,0} - P_{meas,0})A_{U,0}}{P_{meas} - P_{ref}} \quad (4.1.2)$$

where A_L and A_U are the effective areas of the lower and upper PCA part respectively and the 0 subscript is used to denote the corresponding quantities during the load cell zeroing. Assuming that the lubrication pressure is constant and the zeroing pressures at the upper and lower part are equal to the reference pressure the combined effective area of the whole PCA reduces to:

$$A_{total} = \frac{P_{meas}A_U - P_{ref}A_{U,0}}{P_{meas} - P_{ref}} - \frac{P_{lub}(A_U - A_{U,0})}{P_{meas} - P_{ref}} \quad (4.1.3)$$

In Fig. 16 the effective areas of the whole FPG assemblies of PTB, SP and INRIM calculated from the corresponding kinetic results that have been provided earlier are presented, where the zeroing pressure was assumed to be 1 Pa in absolute mode and 100001 Pa in gauge mode. In all three configurations the effective area slightly deviates around a constant value when the FPG operates under gauge mode. For the FPG of PTB the average effective area in gauge mode is 9.806072 cm^2, while for the FPGs of SP and INRIM their respective average effective areas are 9.805072 cm^2 and 9.805185 cm^2. In absolute mode the effective area of PTB's FPG is 9.806011 cm^2 at 5 Pa and tends to a constant value of 9.806065 cm^2 at higher measurement pressures. The same qualitative behavior for the absolute mode is present in the SP and INRIM FPG assemblies. The effective areas of the two latter assemblies are 9.805269 cm^2 and 9.805246 cm^2 at 5 Pa and tend to a constant value of 9.805120 cm^2 and 9.805195 cm^2 respectively. As mentioned earlier, the effective area for the whole PTB FPG is higher due to the slightly larger piston radius. It is also noted, that since in the PTB configuration the gas inside

the piston-cylinder clearance is less rarefied the effective area tends to take a constant value in lower measurement pressures than the assemblies of SP and INRIM.

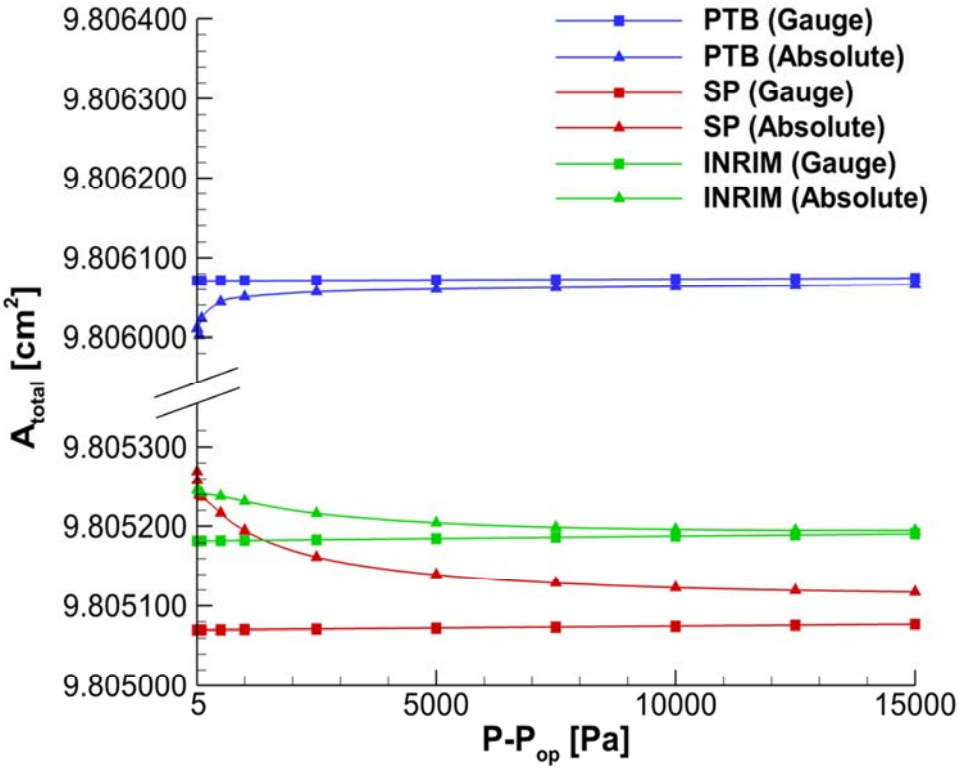

Figure 16: Kinetic results for the effective area for the whole FPG assembly of PTB, SP and INRIM.

4.2 Furness Rosenberg Standard: FRS4

4.2.1 Dimensional and operational data

The representation of the FRS4 gap simulation is shown in Fig. 17. As described in Chapter 2 the lubricating gas flow enters the piston-cylinder gap radially from the top section of the cylinder, flows through the gap and is removed before reaching the reference pressure chamber. The inlet pressure of the gap corresponds to the measurement pressure and in reality it ranges from 100001 Pa up to 103200 Pa in gauge mode and from 1 Pa up to 3200 Pa in absolute mode. However, in the performed simulations a pressure range same as the FRS5 which is up to 111000 Pa in gauge mode and up to 11000 Pa in absolute mode will be investigated.

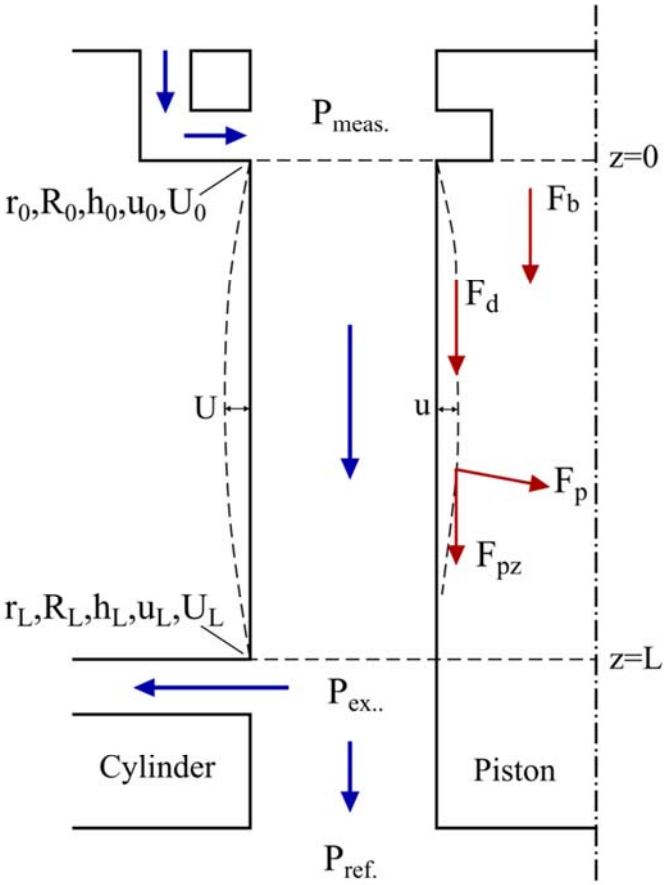

Figure 17: Representation of an FRS4 gap cross section simulation.

The gap outlet pressure corresponds to the exhaust pressure which slightly differs from the reference pressure. However, since estimations of the exhaust pressure are not available for the FRS4 configuration under investigation the reference pressure will be used for the simulation purposes. Thus the outlet pressure is taken to be 100000.01 Pa in gauge mode and 0.01 Pa in absolute mode. In the FRS4 gap the simulating gas is assumed to be dry N_2 at 20 ^{o}C.

In the frame of the second work package of the EMPIR 14IND06 pres2vac project one FRS4 gauge has been dimensionally characterized by CMI (Czech Metrology Institute). The complete dimensional analysis of the FRS4 has been delivered to UTH in order to simulate the gas flow inside the PCA gap. The measurement characteristics of the performed dimensional analysis are presented in Table 13.

Table 13: Measurement and dimensional characteristics of the FRS assembly provided by CMI.

CMI FRS4			
Measurement angles	8	Cyl. measurement length	49.0
Angle interval [deg]	45	Average piston radius [mm]	56.41841
Pist. measurements	2001	Average cylinder radius [mm]	56.45182
Pist. Measurement interval [mm]	0.0230	Average gap inlet [μm]	31.78
Pist. measurement length	46.0	Average gap width [μm]	33.41
Cyl. measurements	2001	Average gap outlet [μm]	34.06
Cyl. Measurement interval [mm]	0.0245	Average piston area [cm2]	99.99807

As shown in Table 13 the measurements have different measuring intervals and lengths for the piston and cylinder. Thus, measurements at the exact same gap height, required for the gas flow simulations, were not available. To circumvent this, numerical treatment has been applied on the provided piston and cylinder measurements in order to provide the required simulation data. In the overlapping 40 mm length of the piston and cylinder measurements 501 nodes were taken with a uniform spacing of 0.08 mm. The piston and cylinder radii in each node were then calculated by performing a linear interpolation between the two adjacent measurements. The original piston and cylinder radii measurements provided by CMI, as well as the interpolated ones used in the gas flow simulations are shown in Fig. 18.

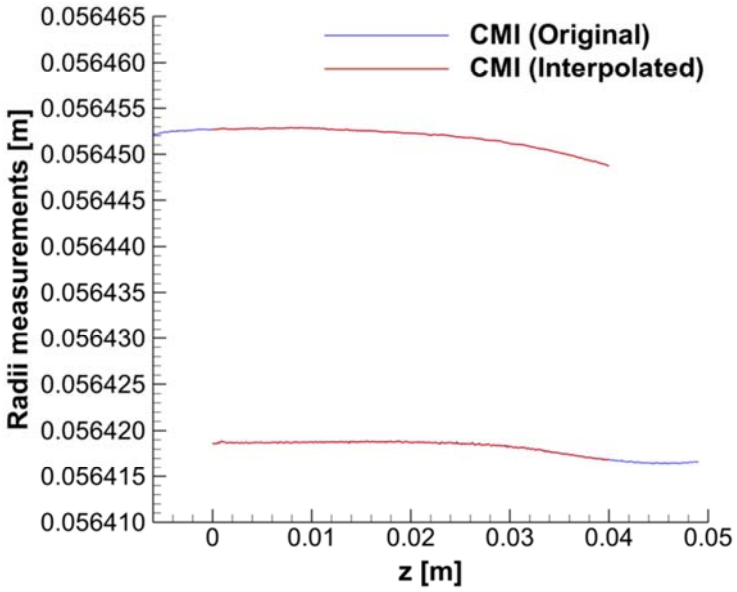

Figure 18: Piston and cylinder radii measurements averaged over all angles as provided by CMI and interpolated.

4.2.2 Effective area: approximate approach

Simulations have been performed to compute the effective area of the FRS dimensionally characterized by CMI based on the approximate approach. In Fig. 19 the effective area calculations for the FRS configuration of CMI based on Dadson theory, Fluent and kinetic theory are provided. Similarly to the FPG, in order to have a uniform representation for the effective areas in the gauge and absolute operation modes all results are presented with respect to $P - P_{op}$ where P is the inlet pressure of the PCA, while P_{op} is set to 100 kPa in gauge mode and 0 Pa in absolute mode. It is observed that, the agreement between Dadson theory and Fluent is excellent in the whole simulation range with a highest relative deviation of 0.24 ppm. In addition, the comparison between Dadson and kinetic results shows discrepancies of 0.74 ppm in gauge mode and up to 27.8 ppm in absolute mode. It is noted that, although the gap of an FRS4 is wider than that of an FPG8601, the operating pressures in absolute mode are orders of magnitude lower, thus justifying the higher discrepancies between kinetic and viscous results.

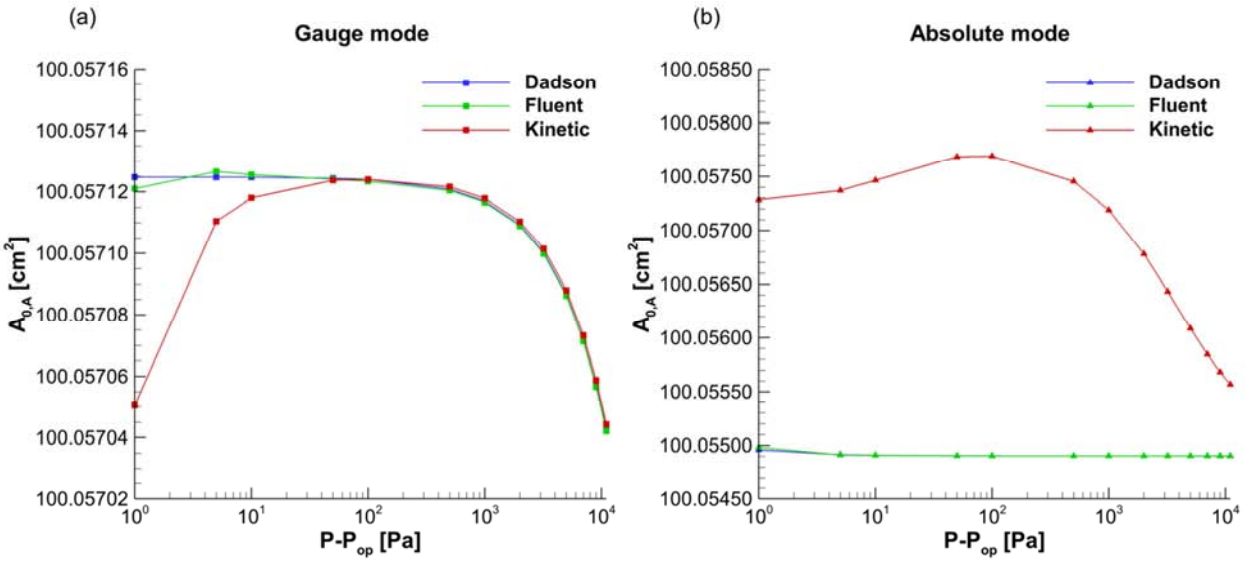

Figure 19: Effective area calculations for the FRS assembly of CMI based on the approximate approach.

In Table 14 the effect of the gas flow and piston variation on the effective area based on kinetic theory is provided. It is shown that, the ratio of the effective area due to the gas flow and the piston variation over the effective area slightly deviates from an average of 581.4 ppm in gauge

mode. In absolute mode the ratio is 583.3 ppm at 1 Pa then it rapidly reaches a peak of 587.4 ppm at 100 Pa and eventually reduces to 566.2 ppm at 11000 Pa.

Table 14: Effect of gas flow and piston radius variation on the effective area for the FRS assembly of CMI based on the approximate approach.

Operation Mode	Gauge			Absolute		
$P - P_{ref}$ [Pa]	$A_{0,A}$ [cm^2]	$A_{2,A}$ [cm^2]	$\frac{A_{2,A}}{A_{0,A}} \cdot 10^6$	$A_{0,A}$ [cm^2]	$A_{2,A}$ [cm^2]	$\frac{A_{2,A}}{A_{0,A}} \cdot 10^6$
1	100.05705	0.056564	581.0	100.05728	0.058365	583.3
10	100.05712	0.058200	581.7	100.05746	0.058546	585.1
100	100.05712	0.058206	581.7	100.05769	0.058773	587.4
1000	100.05712	0.058200	581.7	100.05719	0.058273	582.4
3200	100.05710	0.058184	581.5	100.05643	0.057514	574.8
7000	100.05707	0.058156	581.2	100.05585	0.056928	569.0
11000	100.05704	0.058127	580.9	100.05557	0.056651	566.2

4.2.3 Effective area: effect of measurements

The dimensional measurements of the FRS4 configuration provided by CMI contain significant variations along the PCA engagement length and thus computing the effective area based on the exact approach is prohibitive. However, the two approaches can be compared based on polynomial least squares approximations. The least squares expressions were derived from the interpolated data, by iteratively increasing the degree of the interpolating polynomial upon convergence of the well-known statistics coefficient R^2. In Fig. 20 the piston and cylinder radii measurements of the FRS configuration and the corresponding least squares approximations averaged over all angles are presented. It is observed that the least squares approximations closely represent the real geometry, while the radii variation originating from the surface roughness and uncertainty of dimensional measurement is omitted.

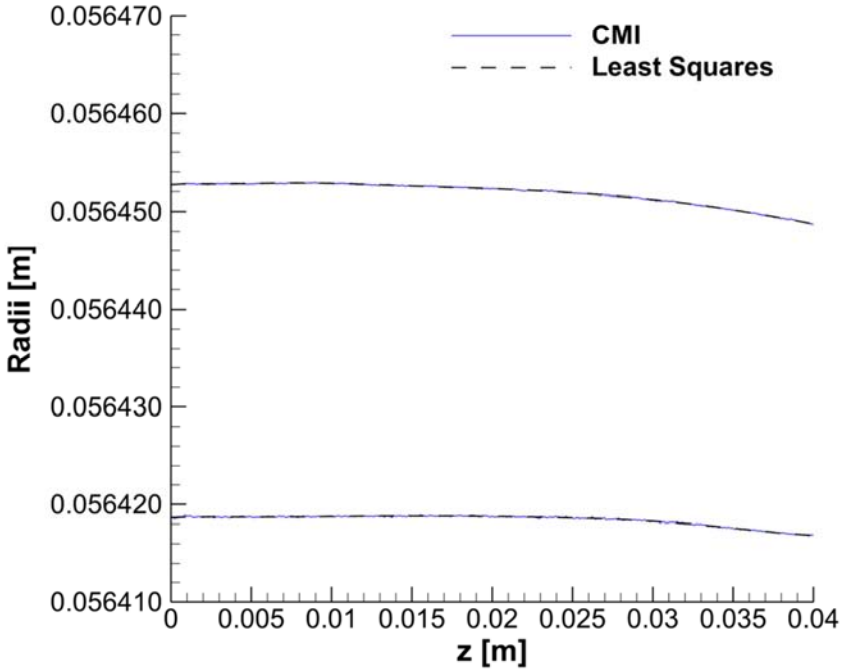

Figure 20: Piston and cylinder radii measurements provided by CMI and corresponding least squares approximations averaged over all angles.

Table 15: Effective area computed by the approximate and exact approaches based on polynomial least squares approximations for the FRS assembly of CMI.

Operation mode	Gauge		Absolute	
$P - P_{ref}$ [Pa]	$A_{0,A}$ [cm^2]	$A_{0,E}$ [cm^2]	$A_{0,A}$ [cm^2]	$A_{0,E}$ [cm^2]
1	100.0570471	100.0570460	100.0572809	100.0572807
10	100.0571154	100.0571153	100.0574630	100.0574629
100	100.0571218	100.0571213	100.0576918	100.0576918
1000	100.0571154	100.0571153	100.0571958	100.0571955
3200	100.0570989	100.0570986	100.0564371	100.0564366
7000	100.0570709	100.0570705	100.0558461	100.0558455
11000	100.0570419	100.0570416	100.0555641	100.0555633

In Table 15 the kinetic results for the effective areas computed based on the least squares radii by the approximate and exact approaches are provided. The average relative deviation between the two approaches is $3.5 \cdot 10^{-3}$ ppm while it reaches a highest value of $1.1 \cdot 10^{-2}$ ppm. The contribution of each effective area part to the overall effective area of the FRS computed by the approximate and exact approaches is presented in Table 16. It is noted that in gauge mode,

where the inlet and outlet pressures are of the order of 100 kPa and the pressure differential tends to zero, the contribution of the piston radius variation to the effective area becomes significantly high. Thus, the implementation of the exact approach based on the real dimensional measurements can provide erroneous results. Finally, it is mentioned that since dimensional and operational data are not available for the lower part of the FRS4 assembly of CMI the total effective area of the PCA cannot be computed. However, preliminary simulations performed by PTB in both upper and lower parts of their FRS5 assembly showed an insignificant contribution of 0.2 ppm to the total effective area.

Table 16: Effective area contributions computed by the approximate and exact approaches based on polynomial least squares approximations for the FRS assembly of CMI.

Operation mode			Gauge		
$P - P_{ref}$ [Pa]	$A_{l,A}$ [cm^2]	$A_{2,A}$ [cm^2]	$A_{l,E}$ [cm^2]	$A_{2,E}$ [cm^2]	$A_{3,E}$ [cm^2]
1	99.998912	0.058135	731.747371	0.059123	-631.749449
10	99.998912	0.058203	162.974594	0.059151	-62.976630
100	99.998912	0.058209	106.313135	0.059153	-6.315167
1000	99.998912	0.058203	100.630277	0.059151	-0.632313
3200	99.998912	0.058187	100.196211	0.059144	-0.198257
7000	99.998912	0.058158	100.089105	0.059133	-0.091167
11000	99.998912	0.058129	100.056308	0.059122	-0.058388
Operation mode			Absolute		
$P - P_{ref}$ [Pa]	$A_{l,A}$ [cm^2]	$A_{2,A}$ [cm^2]	$A_{l,E}$ [cm^2]	$A_{2,E}$ [cm^2]	$A_{3,E}$ [cm^2]
1	99.998912	0.058368	99.998976	0.059218	-0.000913
10	99.998912	0.058551	99.998919	0.059292	-0.000748
100	99.998912	0.058779	99.998913	0.059364	-0.000585
1000	99.998912	0.058283	99.998912	0.059159	-0.000876
3200	99.998912	0.057525	99.998912	0.058894	-0.001370
7000	99.998912	0.056934	99.998912	0.058707	-0.001774
11000	99.998912	0.056652	99.998912	0.058619	-0.001968

Chapter 5: Concluding remarks

In the present work a variety of numerical tools and approaches for modeling the gas flow inside the gap of piston gauges and the computation of the effective area has been presented and validated. The gas flow inside the piston cylinder gap has been modeled based on both viscous and kinetic theory. For the viscous modeling, an in-house developed code based on one dimensional Dadson theory has been used, along with the commercial software ANSYS Fluent for a two dimensional study. The implementation of commercial software for a two dimensional investigation does not only complement the results of the one dimensional approach but also acts as a validation tool. Furthermore, for the kinetic modeling an in-house code has been developed based on a robust kinetic database that provides the required dimensionless mass flow rates with respect to the dimensional data of the gap and the gas rarefaction.

In the framework of the EMPIR 14IND06 pres2vac project three FPG8601 configurations and one FRS4 configuration have been dimensionally characterized by their respective National Metrology Institutes. The dimensional data were provided to UTH and the described modeling tools were implemented to determine the pressure distribution inside the piston cylinder gaps and to compute the effective areas of the four configurations. The comparison between the two viscous implementations show an excellent agreement in all configurations, while as expected viscous and kinetic results deviate, especially under absolute mode operating conditions. In addition, Dadson and kinetic theory results have been compared with computations performed by PTB for the effective area of their FPG configuration. The agreement was good for the kinetic results and satisfactory for the viscous results. Moreover, effective area computations from least square approximations of the real dimensional data were provided in order to have an appropriate comparison between the approximate and exact approaches. Thus it was shown that, the two approaches deviate due to numerical error introduced in the differentiation of the piston radius.

It is believed that the present work has both scientific interest and technological impact and it is hoped reduce the uncertainties in pressure measurements performed by non-rotating piston gauges. Future extension of this work will be the simulation of one FRS5 configuration which has been already dimensionally characterized by PTB. The simulation of the FRS5 will also provide an indication of the piston lower part effect on the total effective area of the FRS4

configuration. In addition, the work of this thesis can be extended by investigating the effect of the exhaust pressure in the FRS4 configuration and the effect of piston displacement in both FRS4 and FRS5 configurations.

References

[1]: M. E. Himbert, “A brief history of measurement”, Eur. Phys. J. Special Topics, 172, 25–35, 2009.

[2]: H. Czichos (ed.), Handbook of Metrology and Testing, Second Edition, Springer, 2011.

[3]: French College of Metrology, “Metrology in Industry – The Key for Quality”, ISTE Ltd., 2006.

[4]: G. Molinar, “Historical perpectives of high pressure metrology using pressure gauges”, PTB-Mitteilungen 5th CCM Int. Conf. Pressure and Vacuum Metrology, 121, 266-269, 2011.

[5]: A. Ooiwa, M. Ueki, Development of novel air piston gauge for medium and fine differential pressure measurement, Vacuum, 44, 603-605, 1993.

[6]: A. Ooiwa, Novel nonrotational piston gauge with weight balance mechanism for measurement for small differential pressures, Metrologia, 30, 607-610, 1993.

[7]: C. G. Rendle, H. Rosenberg, A large area piston gauge for differential and gauge pressure from zero to 3.2 kPa, 30, 611-613, 1993/1994.

[8]: C. G. Rendle, H. Rosenberg, New absolute pressure standard in the range 1 Pa to 7 kPa, Metrologia, 36, 613-615, 1999.

[9]: Th. Bock, H. Ahrendt, K. Jousten, “Reduction of the uncertainty of the PTB vacuum pressure scale by a new larege area non-rotating piston gauge”, Metrologia, 46, 389-396, 2009.

[10]: M. Knudsen, Die Molekularstroemung der Gase durch Offnungen und die Effusion, Annalen der Physik, 3F33(5), 999-1016, 1909.

[11]: Shen Ching, Rarefied Gas Dynamics, Fundamentals, Simulations and Micro Flows, 2005.

[12]: Sone, Yoshio. Molecular Gas Dynamics, Theory, Techniques and Applications. 2007.

[13]: G.A. Bird, Molecular Gas Dynamics. 1976.

[14]: Cercignani, C. The Boltzmann equation and its Applications. 1988.

[15]: Bhatnagar P.L., Gross E.P., Krook. M. “A model for Collision Processes in Gases. I. Small Amplitude Processes in Charged and Neutral One-Component Systems.” Physical Review (1954): 94(3) 511-525.

[16]: Shakhov, E.M. “Generalization of the Krook kinetic relaxation equation.” Fluid Dyn. (1968): 3(5) 95-96.

[17]: Holway, L.H. Approximation procedure for kinetic theory. PhD thesis, Harvard University, 1963.

[18]: Holway, L.H. "New statistical models for kinetic theory." Physics of Fluids (1966): 9: 1658-1673.

[19]: Rykov, V.A. “Model Kinetic Equations for a Gas with Rotational Degrees of Freedom.” Izv. Akad. Nauk. SSSR. Mekh. Zhidk. Gaza. (1975): (6), 701-115.

[20]: McCormack, F.J. "Construction of linearized kinetic models for gaseous mixtures and molecular gases." Physics of Fluids (1973): 16: 2095.

[21]: G. A. Bird, Monte Carlo simulation of gas flows, Annual Review of Fluid Mechanics, 10, 11-31, 1978.

[22]: K. Jousten, Handbook of Vacuum Technology, Second Edition, Wiley-VCH, 2016.

[23]: W. Boyes (ed.), Instrumentation Reference Book, Fourth Edition, Butterworth-Heinemann, 2009.

[24]: R. M. Besançon (ed.), “Vacuum Techniques”. The Encyclopedia of Physics, Third Edition, Van Nostrand Reinhold, New York, 1990.

[25]: R. S. Dadson, S. Lewis and G. N. Peggs, The Pressure Balance: Theory and Practice, HSMO, 1982.

[26]: G. Molinar, M. Bergolio, W. Sabuga, P. Otal, G. Ayyildiz, J. Verbeek, P.Farar, “Calculation of effective area A0 for six piston–cylinder assemblies of pressure balances. Results of the EUROMET Project 740”, Metrologia, 42, 197-201, 2005.

[27]: K. Jain, W. Bowers, J. W. Schmidt, “A Primary Dead-Weight Tester for Pressures (0.05-1.0) MPa”, J. Res. Natl. Inst. Stand. Technol., 108(2), 135-145, 2003.

[28]: Y. Yang, J. Yue, “Calculation of Effective Area for the NIM Primary Pressure Standards”, PTB-Mitteilungen 5th CCM Int. Conf. Pressure and Vacuum Metrology, 121, 266-269, 2011.

[29]: W. Sabuga, “Pressure measurements in gas media up to 7.5 MPa for the Boltzmann constant redetermination”, PTB-Mitteilungen 5th CCM Int. Conf. Pressure and Vacuum Metrology, 121, 247-255, 2011.

[30]: ANSYS Academic Research, Release 16.2, Help System, FLUENT Theory Guide, ANSYS, Inc.

[31]: J. W. Schmidt, B. E. Welch, C. D. Ehrlich, “Gas and mode, vertical and rotational effects with a three piston gauge apparatus”, Metrologia, 30, 599-602, 1993/94.

[32]: J. W. Schmidt, B. E. Welch, C. D. Ehrlich, “Operational mode and gas species effects on rotational drag in pneumatic dead weight pressure gauge”, Meas. Sci. Technol., 4, 26–34, 1993.

[33]: J. W. Schmidt, S. A. Tison, C. D. Ehrlich, “Model for drag forces in the crevice of piston gauge in the viscous-flow and molecular-flow regime”, Metrologia 36, 565–70, 1999

[34]: J. W. Schmidt , Y. Cen, R. G. Driver, J. W. Bowers, J. C. Houck, S. A. Tison, C. D. Ehrlich, “A primary pressure standard at 100 kPa”, Metrologia, 36, 525–529, 1999.

[35]: J. W. Schmidt, K. Jain, A. P. Miiller, J. W. Bowers, D. A. Olson, “Primary pressure standards based on dimensionally characterized piston/cylinder assemblies”, Metrologia, 43, 53-59, 2006.

[36]: W. Sabuga, F. Sharipov, T. Priruenrom, Determination of the effective area of piston-cylinder assemblies using rarefied gas flow model, PTB-Mitteilungen 5th CCM Int. Conf. Pressure and Vacuum Metrology, 121, 260-262, 2011.

[37]: F. Sharipov, Y. Yang, J. E. Ricker, J. H. Hendricks, “Primary pressure standard based on piston-cylinder assemblies. Calculation of effective cross sectional area based on rarefied gas dynamics”, Metrologia, 56, 1177-1184, 2016.

[38]: F. Sharipov, Rarefied Gas Dynamics. Fundamentals for Research and Practice, Berlin: Wiley, 2016.

[39]: F. Sharipov, V. Seleznev, “Data on internal rarefied gas flows”, J. Phys. Chem. Ref. Dat, 27, 657–706, 1998.

[40]: G. Breyiannis, S. Varoutis and D. Valougeorgis, “Rarefied gas flow in concentric annular tube: Estimation of the Poiseuille number and the exact hydraulic diameter”, European Journal of Mechanics B/Fluids, 27, 609-622, 2008.

[41]: B. Fornberg, “Generation of Finite Difference Formulas on Arbitrarily Spaced Grids”, Mathematics of Computation, 51, 699-706, 1988.

[42]: S. Chapra, R. Canale, Numerical Methods for Engineers, Sixth Edition, McGraw-Hill, 2009.

Appendix A: Numerical integration and differentiation

As described in Chapter 3 all quantities that appear in the computation of a PCA effective area are functions of the piston radius, the cylinder radius, the pressure inside the gap and their first derivatives. In order to achieve the required accuracy in the calculation of pressure and radii derivatives a set of forward, backward, and central 4^{th} order finite differences is implemented. For a uniform grid the general finite difference scheme can be written as:

$$\left.\frac{df}{dx}\right|_i = \frac{1}{\Delta x}\sum_j c_j f\left(x_j\right) \tag{A.1}$$

where Δx is the grid spacing, $f\left(x_j\right)$ is the value of f at node j and c_j are the finite difference coefficients. The coefficients for the finite differences in the whole computation domain are provided for completeness purposes in Table A.1 [41]:

Table A.2: Finite differences coefficients for a uniform spaced grid.

Computation Node	$i-4$	$i-3$	$i-2$	$i-1$	i	$i+1$	$i+2$	$i+3$	$i+4$
$i=1$	0	0	0	0	-25/12	48/12	36/12	16/12	-3/12
$i=2$	0	0	0	-3/12	-10/12	18/12	-6/12	1/12	0
$3\le i\le N-2$	0	0	1/12	-8/12	0	8/12	-1/12	0	0
$i=N-1$	0	-1/12	6/12	-18/12	10/12	3/12	0	0	0
$i=N$	3/12	-16/12	36/12	-48/12	25/12	0	0	0	0

In order to compute the contribution of the gas flow to the effective area it necessary to integrate the forces exerted on the piston along the piston cylinder engagement length. Furthermore, an integration of the gap height is also required in order to determine the pressure distribution according to Dadson theory. In the present work all numerical integrations are done on a uniform spaced grid by implementing a composite Newton-Cotes quadrature scheme [42]. For a single subinterval $(n=1)$ the integration formula is given as:

$$\int_a^b f(x)\,dx = \frac{\Delta x}{24}\left(9f\left(x_1\right)+19f\left(x_2\right)-5f\left(x_3\right)+f\left(x_4\right)\right) \tag{A.2}$$

The above expression is derived by applying the first and second Simpson rules in an overlapping interval. For an even number of subintervals with $n \geq 2$ the integration formula reduces to the first Simpson's rule expressed as:

$$\int_a^b f(x)\,dx = \frac{\Delta x}{3}\sum_{j=1}^{n/2}\left(f\left(x_{2j-1}\right)+4f\left(x_{2j}\right)+f\left(x_{2j+1}\right)\right) \tag{A.3}$$

Finally for an odd number of subintervals with $n \geq 3$ the integration formula is given by applying the first and second Simpson rules in two disjoint intervals as:

$$\begin{aligned}\int_a^b f(x)\,dx = {} & \frac{\Delta x}{3}\sum_{j=1}^{(n-3)/2}\left(f\left(x_{2j-1}\right)+4f\left(x_{2j}\right)+f\left(x_{2j+1}\right)\right) \\ & +\frac{3\Delta x}{8}\left(f\left(x_{n-2}\right)+3f\left(x_{n-1}\right)+3f\left(x_n\right)+f\left(x_{n+1}\right)\right)\end{aligned} \tag{A.4}$$